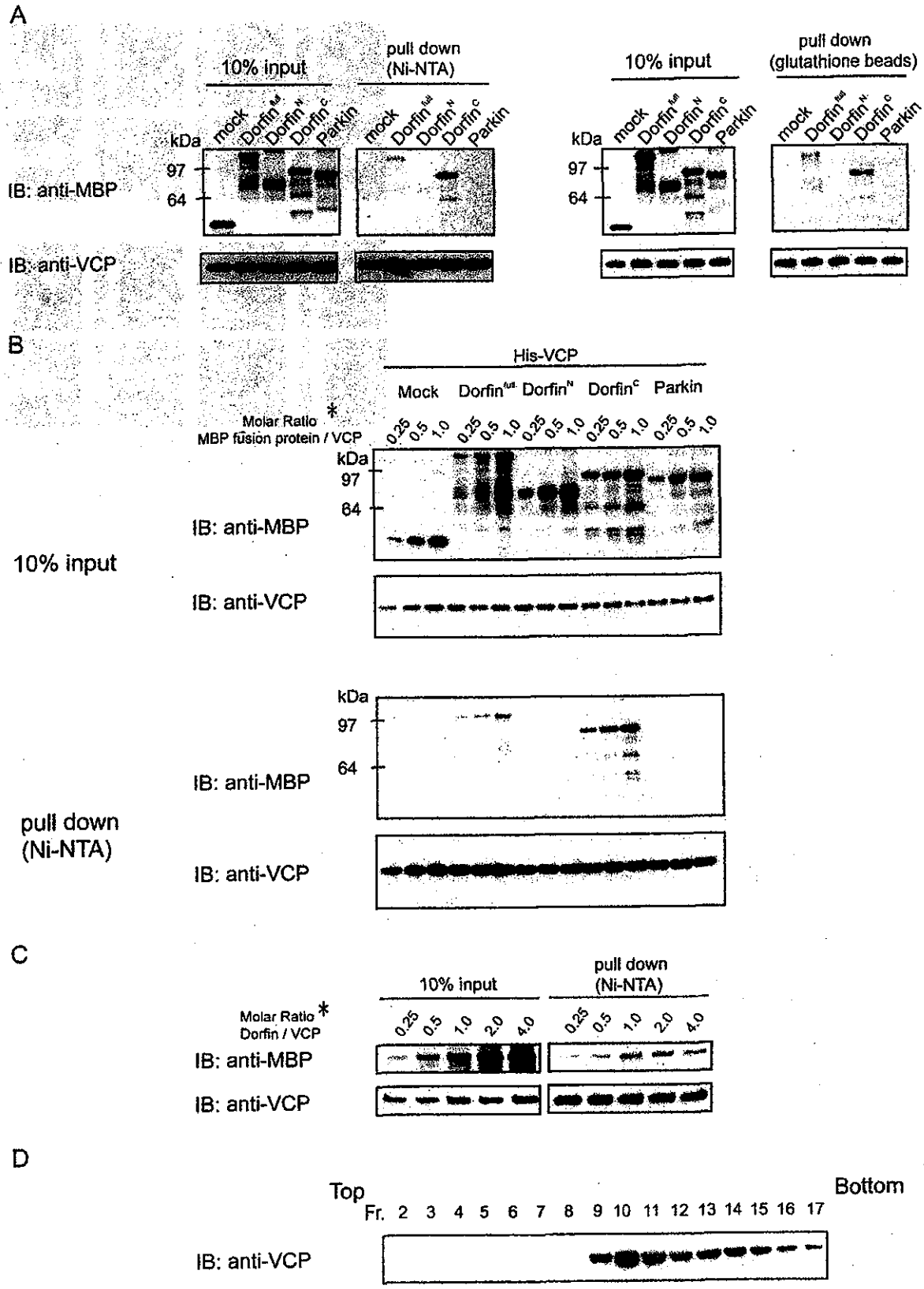


FIG. 3. ***In vitro* interaction between Dorfin and VCP.** *A*, recombinant His- or GST-VCP protein was incubated with MBP-mock, MBP-Dorfin$^{full}$, MBP-Dorfin$^{N}$, MBP-Dorfin$^{C}$, and MBP-Parkin proteins *in vitro*. Two $\mu$g of His- or GST-VCP proteins and MBP fusion proteins at similar molar concentrations to VCP proteins were used for the assays. The amounts of MBP fusion and GST fusion Dorfin derivatives and His-VCP in 10% of the samples used are shown (*10% input*). *NTA*, nitrilotriacetic acid. *IB*, immunoblot. *B*, 2 $\mu$g of His-VCP was incubated with MBP-mock,

binding between Dorfin and VCP and to determine the exact portion of Dorfin that interacts with VCP *in vitro*, we performed pull-down assays using recombinant proteins. Recombinant MBP-Dorfin or its deletion mutants (*i.e.* MBP-Dorfin$^{N}$ and MBP-Dorfin$^{C}$) and the same molar of recombinant His-VCP or GST-VCP were mixed and incubated for 1 h at 4 °C. MBP-mock protein was used as a negative control in these experiments. A small portion of MBP-Dorfin$^{full}$ or Dorfin$^{C}$ (C-terminal substrate-recognizing domain) bound to both His-VCP and GST-VCP, whereas MBP-mock, MBP-Dorfin$^{N}$ (N-terminal RING-IBR domain), and MBP-Parkin did not bind to His-VCP or GST-VCP (Fig. 3*A*). We next determined the number of Dorfins that bind one hexamer of VCP. To investigate this issue, we incubated His-VCP with increasing amounts of MBP-Dorfin$^{full}$, MBP-Dorfin$^{N}$, MBP-Dorfin$^{C}$, MBP-mock, or MBP-Parkin. As shown in Fig. 3*B*, the amount of binding portion of MBP-Dorfin$^{full}$ and -Dorfin$^{C}$ pulled down with His-VCP was not saturated below the even molar ratio. The pull-down experiments using excess amounts of MBP-Dorfin$^{full}$ revealed that MBP-Dorfin$^{full}$ was saturated at the even molar ratio (Fig. 3*C*). As reported previously (15), recombinant His-VCP sedimented in high molecular weight fractions, indicating that it formed a hexamer *in vitro* (Fig. 3*D*). These findings indicated that six Dorfin molecules were likely bind to a VCP complex *in vitro*.

*Subcellular Localization of Dorfin and VCP in HEK293 Cells*—In previous studies, we showed that exogenous and endogenous Dorfin resided perinuclearly and was colocalized with Vimentin in cultured cells treated with a proteasome inhibitor (4). The staining patterns of Dorfin were indistinguishable from those of the aggresome, namely a pericentriolar, membrane-free, cytoplasmic inclusion containing misfolded ubiquitylated proteins packed in a cage of intermediate filaments (4). VCP immunostaining was also observed throughout aggresomes in cultured neuronal cells when induced by treatment with a proteasome inhibitor (15). In order to examine the subcellular localization of Dorfin and VCP, GFP-Dorfin and HA-VCP were co-expressed in HEK293 cells. Without proteasome treatment, GFP-Dorfin-expressing cells showed granular fluorescence in the cytosol, and the HA-VCP-expressing cells showed diffuse and uniform cytoplasmic staining (Fig. 4*A*). Treatment with MG132 (1 μM, 16 h) resulted in accumulation of both GFP-Dorfin and HA-VCP and perinuclear colocalization as a clear large protein aggregate that mimics aggresomes (Fig. 4*B*).

*Colocalization of Dorfin and VCP in the Affected Neurons of ALS and PD*—In previous studies, immunostaining of Dorfin and VCP was independently noted in LBs of PD, and the peripheral staining pattern of both proteins in LBs was similar (7, 23). To confirm the immunoreactivities of Dorfin and VCP in the affected neurons in ALS and PD, we performed a double-labeling immunofluorescence study using a rabbit polyclonal anti-Dorfin antibody (Dorfin-41) and a mouse monoclonal VCP antibody on the postmortem samples of ALS and PD. In the ALS spinal cords, both proteins were colocalized in the LB-like inclusions (Fig. 5, *A–F*). The margin of LBs in PD was intensely immunostained for Dorfin and VCP, and merged images confirmed their strong colocalization (Fig. 5, *G–L*). Dorfin and VCP were also positive in Lewy neurites in the affected neurons of PD (Fig. 5, *M–O*).

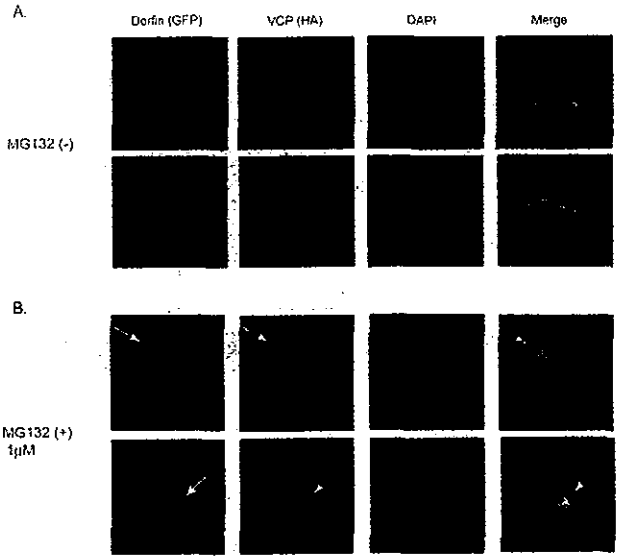


FIG. 4. **Subcellular localization of GFP-Dorfin and HA-VCP in HEK293 cells treated or untreated with a proteasome inhibitor.** GFP-Dorfin and HA-VCP were co-expressed transiently in HEK 293 cells. Cells were treated with (*B*) or without (*A*) 1 μM MG132 for 16 h. HA-VCP was stained with anti-monoclonal HA antibody (12CA5). Nuclei were stained with 4′,6-diamidino-2-phenylindole (*DAPI*). Without the treatment of MG132, GFP-Dorfin was spread through the cytosol, and it appeared like small aggregations. HA-VCP was also seen mainly in the cytosol and partly colocalized with GFP-Dorfin (*A*). After treatment with 1 μM MG132 for 16 h, both GFP-Dorfin and HA-VCP showed perinuclear accumulation and colocalization and appeared as clear large protein aggregates (*B*; *arrows*).

*Dorfin Ubiquitylates Mutant SOD1 in Vivo*—Unlike the wild-type form, mutant SOD1 proteins are rapidly degraded by the ubiquitin-proteasome system. Consistent with our previous results (5), SOD1$^{G93A}$ and SOD1$^{G85R}$ were polyubiquitylated, and co-expression with FLAG-Dorfin$^{WT}$ enhanced polyubiquitylation of these mutant SOD1s compared with co-expression with FLAG-BAP, a negative control construct (Fig. 6*A*). Boiling with 1% SDS-containing buffer did not change the level of ubiquitylated mutant SOD1, indicating that mutant SOD1 itself was ubiquitylated by Dorfin (Fig. 6*B*). We also performed the same *in vivo* ubiquitylation assay using Neuro2a cells to examine for E3 activity of Dorfin in neuronal cells. The enhanced polyubiquitylation of these mutant SOD1s by Dorfin was observed in Neuro2a cells as well as in HEK293 cells (Fig. 6*C*). FLAG-Dorfin$^{C132S/C135S}$ did not enhance polyubiquitylation of mutant SOD1s, indicating that this RING finger mutant form was functionally inactive (Fig. 6*D*).

*VCP$^{K524A}$ Suppresses the E3 Activity of Dorfin*—VCP has two ATPase binding domains (D1 and D2). A D2 domain mutant, VCP$^{K524A}$, induces cytoplasmic vacuoles, which mimics vacuole formation seen in the affected neurons in various neurodegenerative diseases (11, 15). The D2 domain represents the major ATPase activity and is essential for VCP function (11). The ATPase activity of VCP$^{K524A}$ is much lower than that of VCP$^{WT}$, and VCP$^{K524A}$ caused accumulation of polyubiquitylated proteins in the nuclear and membrane fractions together with elevation of ER stress marker proteins due to ERAD

MBP-Dorfin$^{full}$, MBP-Dorfin$^{N}$, MBP-Dorfin$^{C}$, and MBP-Parkin with increasing amounts (molar ratio to VCP: 0.25, 0.5, and 1.0). The amounts of MBP fusion Dorfin derivatives and His-VCP in 10% of the samples used are shown (10% input). *C*, 2 μg of His-VCP was incubated with MBP-Dorfin$^{full}$ with increasing amounts (molar ratio to VCP: 0.25, 0.5, 1, 2, and 4). The amounts of MBP-Dorfin$^{full}$ and His-VCP in 10% of the samples used are shown (*10% input*). *D*, His-VCP protein (0.5 μg) was fractionated by 10–40% glycerol gradient centrifugation followed by separation into 30 fractions using a fraction collector. Immunoblotting using anti-VCP antibody was performed on the selected fractions (fractions 2–17). *, The molar ratio was calculated by the amount of VCP monomers, not VCP complexes.

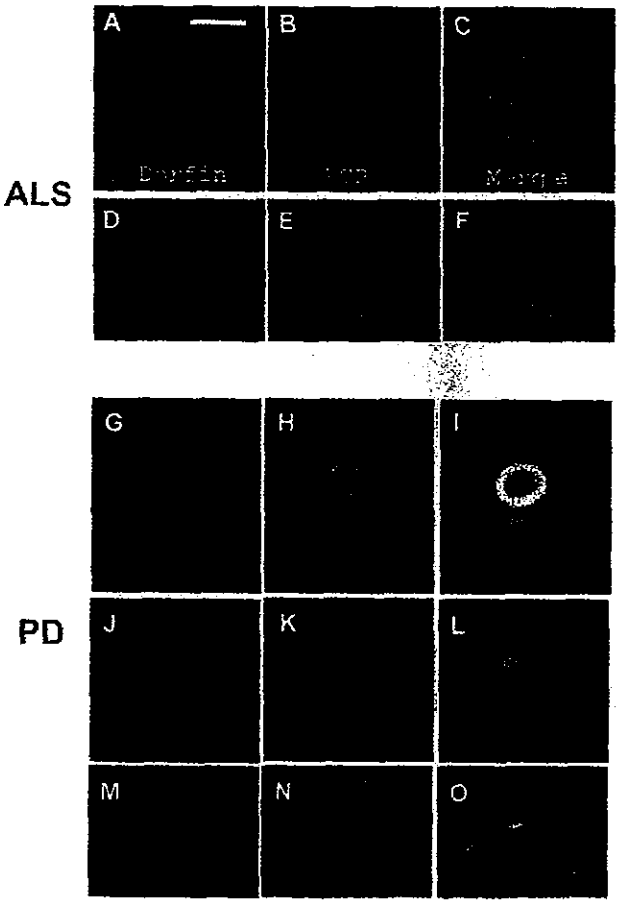


FIG. 5. **Colocalization of Dorfin-41 immunoreactivity with VCP in neuronal inclusions in ALS and PD.** Sections were doubly labeled with anti-Dorfin-41 antiserum and monoclonal VCP antibody and analyzed with a laser-scanning confocal microscope. The *left panels* (*green*) correspond to Dorfin, *middle panels* (*red*) correspond to VCP, and *right panels* correspond to merged images; structures in *yellow* indicate colocalization. Colocalization of Dorfin and VCP is seen in LB-like inclusions in motor neurons of the spinal cord of ALS (*A–F*). Dorfin is also colocalized with VCP in the margin of LBs (*G–I*), premature LBs (*J–L*), and Lewy neurites (*M–O*) in the nigral neurons of PD. *Scale bars*, 20 μm (*A–L*) and 10 μm (*M–O*).

inhibition, whereas its expression level, localization, and complex formation were indistinguishable from those of $VCP^{WT}$ (11). In order to examine the functional effect of VCP on Dorfin, $VCP^{WT}$, $VCP^{K524A}$, or LacZ was co-expressed with $SOD1^{G85R}$, FLAG-Dorfin, and HA-Ub in HEK293 cells. Co-expression with $VCP^{K524A}$ showed a marked decline of polyubiquitylation of $SOD1^{G85R}$ compared with co-expression with $VCP^{WT}$ or LacZ (Fig. 7*A*, *top* and *middle*). Since Dorfin physically interacts with mutant SOD1s (5), we next investigated whether this decline of polyubiquitylation of $SOD1^{G85R}$ was mediated by reduced affinity between $SOD1^{G85R}$ and Dorfin. Immunoprecipitation by anti-FLAG antibody showed that $VCP^{K524A}$ did not change affinity between $SOD1^{G85R}$ and Dorfin (Fig. 7*A*, *bottom*). Neither $VCP^{WT}$ nor $VCP^{K524A}$ changed the level of polyubiquitylation protein in the total lysate (Fig. 7*B*). To clarify whether this negative effect of $VCP^{K524A}$ is specific for Dorfin, we assessed the autoubiquitylation of FLAG-Parkin in the presence of $VCP^{WT}$, $VCP^{K524A}$, or LacZ. Co-expression of $VCP^{K524A}$ did not decrease autoubiquitylation of FLAG-Parkin compared with co-expression of LacZ or $VCP^{WT}$ (Fig. 7*C*). We performed the same experiments using Neuro2a cells to see whether $VCP^{K524A}$ suppress the E3 activity of Dorfin in neuronal cells. The marked decline of polyubiquitylation of $SOD1^{G85R}$ by $VCP^{K524A}$ expression was also seen in Neuro2a cells (Fig. 7*D*).

## DISCUSSION

UBIs in the affected neurons are histopathological hallmarks in various neurodegenerative disorders (8). Dorfin is an E3 ligase, which can ubiquitylate mutant SOD1s and synphilin-1 (5, 24). These substrates and Dorfin were identified in UBIs in various neurodegenerative diseases, such as LB-like inclusions in ALS and LBs in PD and dementia with Lewy bodies (7). This finding suggests that Dorfin may play a crucial role in the process of generating inclusions in the affected neurons. In the present study, we identified VCP as one of the Dorfin-associated proteins using mass spectrometry, and VCP-Dorfin physical interaction was confirmed by an immunoprecipitation experiment using FLAG-Dorfin and HA-VCP overexpressed in HEK293 cells (Fig. 1*A*). VCP is an essential and highly conserved protein of the AAA-ATPase family, which is considered to have diverse cellular functions, such as membrane fusion (25–27), nuclear trafficking (28), cell proliferation (29, 30), and the ERAD pathway (18–22). Many reports have implied that VCP is involved in the pathogenesis of various neuromuscular diseases. VCP has been implicated as a factor that modifies the progress of polyglutamine-induced neuronal cell death (15). In addition, histopathological studies revealed positive staining for VCP in UBIs in PD and ALS with dementia (23). VCP is also associated with MJD protein/atxin-3, in which abnormal expansion of polyglutamine tracts causes Machado-Joseph disease/spinocerebellar ataxia type 3 (31). VCP is also required for the degradation of ataxin-3 in collaboration with E4B/Ufd2a, a ubiquitin chain assembly factor (E4) (32). Recent studies have indicated that missense mutations in the VCP gene cause inclusion body myopathy associated with Paget's disease of bone and frontotemporal dementia, which is characterized by the presence of vacuoles in the cytoplasm in muscle fibers (33).

Our results showed that endogenous Dorfin formed a 400–600-kDa complex in various tissues and various cultured cells (Fig. 1*B*). Dorfin is a ~91-kDa protein; therefore, this high $M_r$ complex should include Dorfin-associated proteins, although the possibility that Dorfin itself oligomerizes in the cell cannot be excluded. Glycerol gradient centrifugation analysis and immunoprecipitation experiments in the present study showed that endogenous Dorfin interacted with endogenous VCP in a complex of approximately 600 kDa, possibly including a Dorfin molecule and a hexametric form of VCP (Fig. 1*C*).

The first RING mutant of Dorfin, in which Cys at positions 132 and 135 changed to Ser, was prepared. This mutant Dorfin, $Dorfin^{C132S/C135S}$, could not ubiquitylate mutant SOD1s (Fig. 6*D*). Glycerol gradient centrifugation analysis revealed that $Dorfin^{C132S/C135S}$ did not form a high $M_r$ complex, whereas exogenous wild type Dorfin ($Dorfin^{WT}$) formed a high $M_r$ complex similar to endogenous Dorfin (Fig. 2*A*). Furthermore, an immunoprecipitation experiment using $Dorfin^{WT}$ and $Dorfin^{C132S/C135S}$ revealed that $Dorfin^{WT}$ could interact with VCP, whereas $Dorfin^{C132S/C135S}$ could not (Fig. 2*B*).

Our *in vitro* study using recombinant proteins showed that full-length ($MBP\text{-}Dorfin^{full}$) and the C terminus of Dorfin ($MBP\text{-}Dorfin^{C}$) directly interacted with VCP, whereas the $MBP\text{-}Dorfin^{N}$ mutant, containing the entire RING finger domain (amino acid residues 1–367), did not bind to VCP (Fig. 3*A*). This finding was unexpected, since *in vivo* binding analysis suggested that Dorfin could interact with VCP at the RING finger domain. It is plausible that certain structural changes in $Dorfin^{C132S/C135S}$ might render the C-terminal VCP-binding portion incapable of accessing VCP molecules. This may explain the result that $Dorfin^{C132S/C135S}$ did not form a high $M_r$ complex.

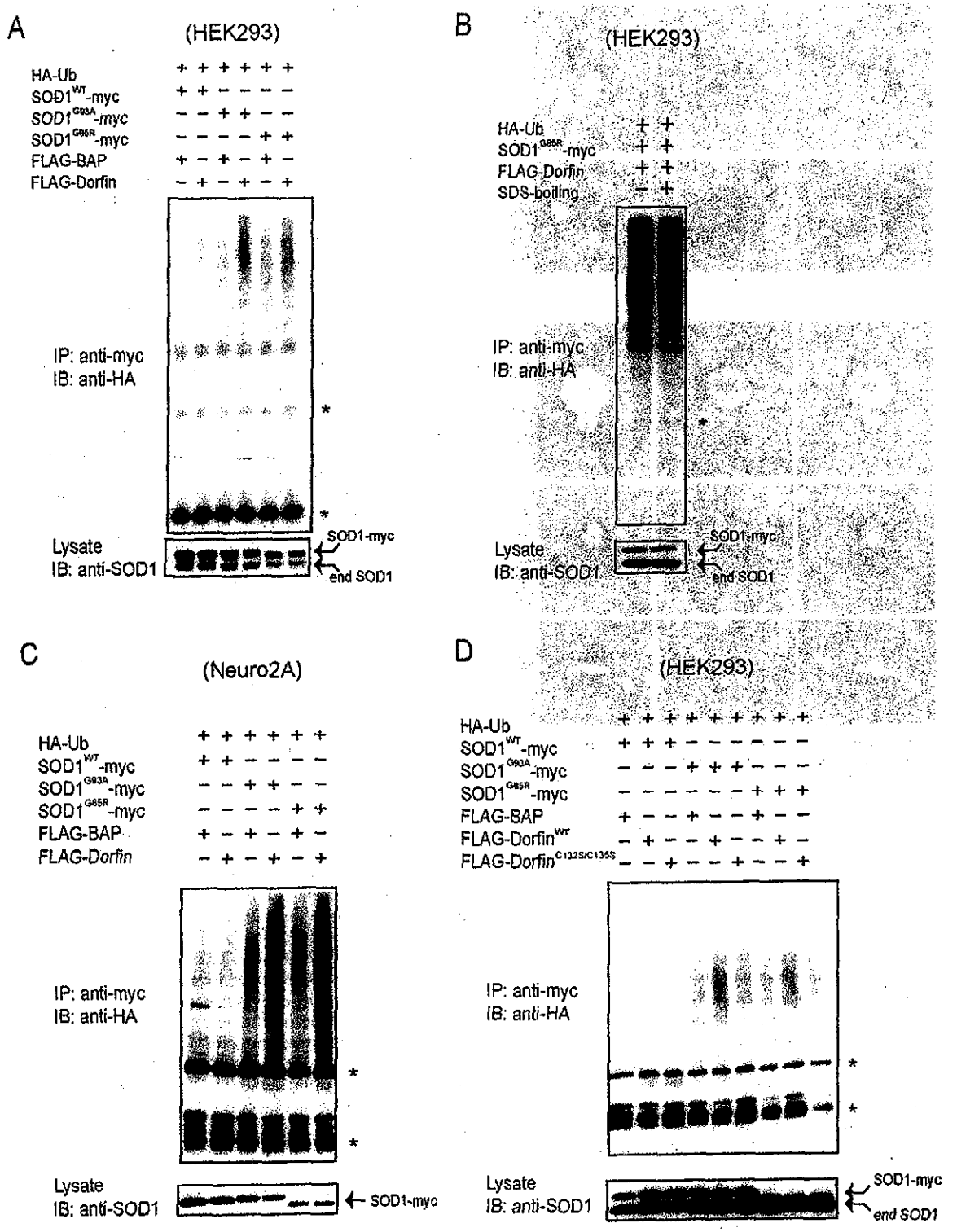


*FIG. 6.* **Dorfin ubiquitylates mutant SOD1s *in vivo*.** *A*, increased ubiquitylation of mutant SOD1 proteins by overexpression of Dorfin. HEK293 cells were co-transfected with $SOD1^{WT}$-Myc, $SOD1^{G93A}$-Myc, or $SOD1^{G85R}$-Myc and HA-Ub with or without FLAG-Dorfin. FLAG-bovine alkaline phosphatase (*BAP*) was used as a negative control. Immunoprecipitation (*IP*) was performed with Myc antibody (9E10). *IB*, immunoblotting. *B*, *SDS boiling* was performed prior to immunoprecipitation. To examine covalently ubiquitylated molecules, the cell lysate was boiled with the buffer containing 1% SDS for 5 min. Immunoprecipitation with Myc antibody (9E10) showed that the SDS-boiling procedure did not change polyubiquitylation level of $SOD1^{G85R}$-Myc by Dorfin. *C*, increased ubiquitylation of mutant SOD1 proteins by overexpression of Dorfin in Neuro2a cells. The same *in vivo ubiquitylation assay* as in *A* was performed using Neuro2a cells. *D*, $Dorfin^{C132S/C135S}$ ($Dorfin^{C132S/C135S}$) did not have E3 activity on mutant SOD1. HEK293 cells were co-transfected with $SOD1^{WT}$-Myc, $SOD1^{G93A}$-Myc, or $SOD1^{G85R}$-Myc and HA-Ub with FLAG-$Dorfin^{WT}$ or FLAG-$Dorfin^{C132S/C135S}$. The *asterisks* indicate IgG light and heavy chains.

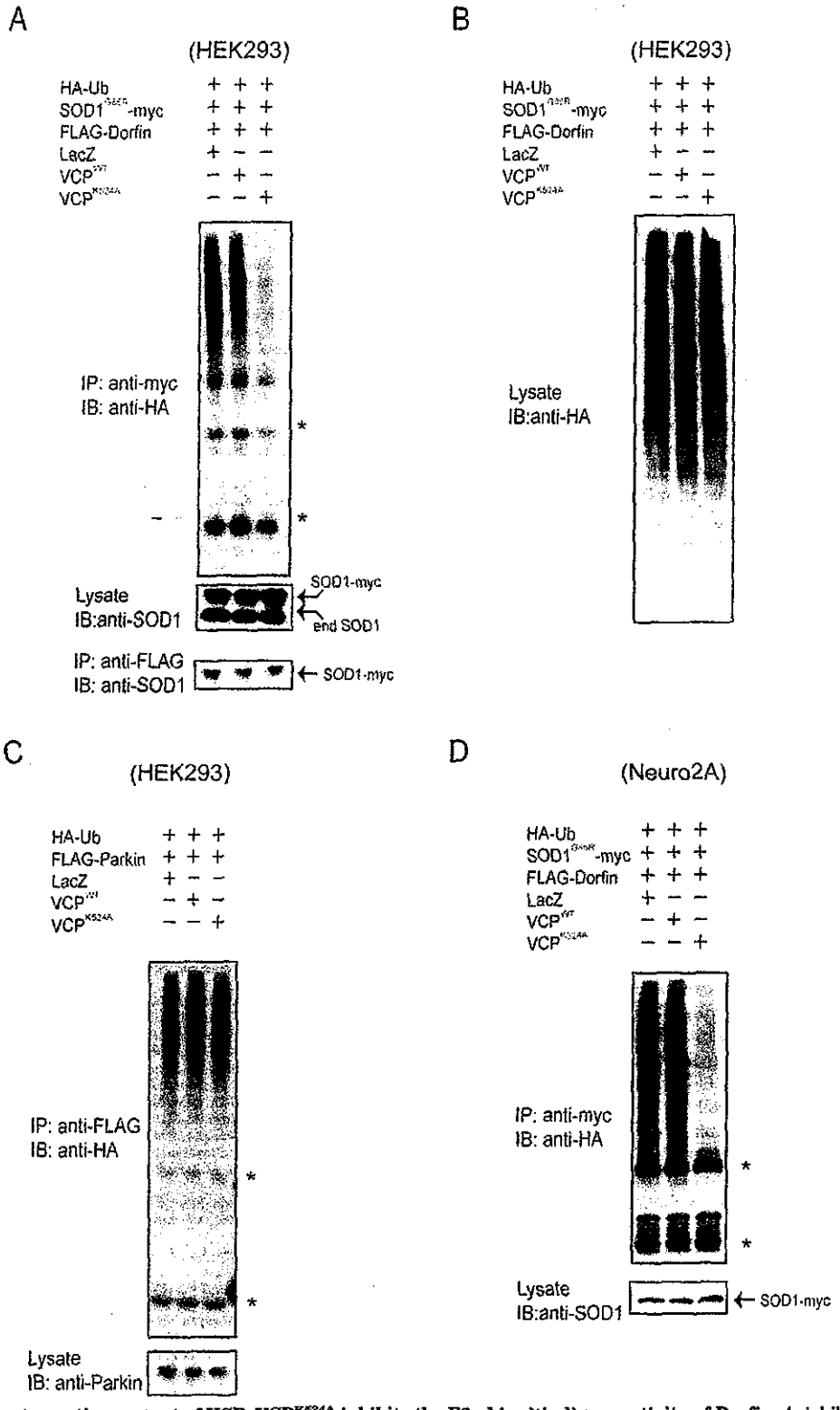


FIG. 7. **A dominant negative mutant of VCP, VCP$^{K524A}$ inhibits the E3 ubiquitin ligase activity of Dorfin.** *A*, inhibition of dominant negative form mutant VCP$^{K524A}$ on the E3 ubiquitin ligase activity of Dorfin. HEK293 cells were co-transfected with SOD1$^{G85R}$-Myc, HA-Ub, FLAG-Dorfin, and VCP$^{WT}$, VCP$^{K524A}$, or LacZ. Immunoprecipitation (*IP*) was performed with Myc antibody (9E10) and FLAG antibody (M2). *IB*, immunoblotting. *B*, neither VCP$^{WT}$ nor VCP$^{K524A}$ changed the level of total polyubiquitylated protein in the cell lysate. Ten percent of the volume of HEK293 cells used in *A* was subjected to immunoblotting using anti-HA (12CA5) antibody. *C*, autoubiquitylation of FLAG-Parkin was not influenced by the dominant negative form VCP$^{K524A}$. HEK293 cells were co-transfected with FLAG-Parkin, HA-Ub, and VCP$^{WT}$, VCP$^{K524A}$, or LacZ. Immunoprecipitation with FLAG antibody (M2) was performed. *D*, inhibition of VCP$^{K524A}$ on E3 ubiquitin ligase activity of Dorfin in Neuro2a cells. Neuro2a cells were co-transfected with SOD1$^{G85R}$-Myc, HA-Ub, FLAG-Dorfin, and VCP$^{WT}$, VCP$^{K524A}$, or LacZ. Immunoprecipitation was performed using Myc antibody (9E10) and FLAG antibody (M2). The *asterisks* indicate IgG light and heavy chains.

The amount of Dorfin bound with VCP was saturated at even molar ratio *in vitro* (Fig. 3, *B* and *C*). Since VCP exists as a homohexamer (Fig. 3*D*), the *in vivo* observed size of ~600 kDa appears to be too small for the Dorfin-VCP complex if one VCP molecule binds to more than one Dorfin as shown in *in vitro* experiments. However, it is noteworthy that the size of molecules estimated by glycerol density gradient centrifugation analysis used in this study is not accurate and sufficient to discuss the molecular interaction of Dorfin and VCP in the cells. To date, various adaptor proteins, with which VCP forms multiprotein complexes, have been identified, such as Npl4, Ufd1 (18, 20), Ufd2 (34), Ufd3 (35), p47 (36), or SVIP (37). Although our *in vitro* study showed direct physical interaction between Dorfin and VCP, the environment with those adaptor proteins might reflect *in vivo* conditions. This also may explain the apparent discrepancy of the Dorfin-VCP binding fashions between *in vivo* and *in vitro* analyses.

Treatment with a proteasomal inhibitor causes the translocation of endogenous VCP and Dorfin to the aggresome in cultured cells (4, 15). Our results showed that these two proteins indeed colocalized perinuclearly in the aggresome following treatment with a proteasomal inhibitor (Fig. 4). Furthermore, we were able to demonstrate both Dorfin and VCP immunoreactivities in LB-like inclusions in ALS and LBs in PD (Fig. 5). In the majority of LBs, indistinguishable peripheral staining patterns were observed with both anti-Dorfin and anti-VCP antibodies. These results confirmed that both Dorfin and VCP are associated with the formation processes of aggresomes and inclusion bodies through physical interaction.

We showed here that co-expression of $VCP^{K524A}$ resulted in a marked decrease of ubiquitylation activity of Dorfin compared with co-expression of $VCP^{WT}$ or control. On the other hand, $VCP^{K524A}$ failed to decrease autoubiquitylation activity of Parkin. $VCP^{K524A}$ did not change the level of polyubiquitylated protein accumulation in the cell lysate in this study (Fig. 7). Knockdown experiments using the RNA interference technique showed accumulation of polyubiquitylated proteins (38). Combined with the observation that inhibition of VCP did not decrease the general accumulation of polyubiquitylated proteins, our results indicated that the E3 regulation function of VCP may be specific to certain E3 ubiquitin ligases such as Dorfin. VCP is an abundant protein that accounts for more than 1% of protein in the cell cytosol and is known to have various chaperone-like activities (39); therefore, it may function as a scaffold protein on the E3 activity of Dorfin. The localization of Dorfin and VCP in UBIs in various neurodegenerative disorders indicates the involvement of these proteins in the quality control system for abnormal proteins accumulated in the affected neurons in neurodegenerative disorders.

Since the unfolded protein response and ERAD are dynamic responses required for the coordinated disposal of misfolded proteins (40), the ERAD pathway can be critical for the etiology of neuronal cell death caused by various unfolded proteins. VCP is required for multiple aspects of the ERAD system by recognition of polyubiquitylated proteins and translocations to the 26 S proteasome for processive degradation through the VCP-Npl4-Ufd1 complex (18, 41). Our results suggest the involvement of Dorfin in the ERAD system, which is related to the pathogenesis of neurodegenerative disorders, such as PD or Alzheimer's disease. Further study including Dorfin knockout and/or knockdown models should examine the pathophysiology of Dorfin in association with the ERAD pathway or other cellular functions. Such studies should enhance our understanding of the pathogenetic role of Dorfin in neurodegenerative disorders.

REFERENCES


1. Julien, J. P. (2001) *Cell* **104,** 581–591
2. Rowland, L. P., and Shneider, N. A. (2001) *N. Engl. J. Med.* **344,** 1688–1700
3. Ishigaki, S., Niwa, J., Ando, Y., Yoshihara, T., Sawada, K., Doyu, M., Yamamoto, M., Kato, K., Yotsumoto, Y., and Sobue, G. (2002) *FEBS Lett.* **531,** 354–358
4. Niwa, J., Ishigaki, S., Doyu, M., Suzuki, T., Tanaka, K., and Sobue, G. (2001) *Biochem. Biophys. Res. Commun.* **281,** 706–713
5. Niwa, J., Ishigaki, S., Hishikawa, N., Yamamoto, M., Doyu, M., Murata, S., Tanaka, K., Taniguchi, N., and Sobue, G. (2002) *J. Biol. Chem.* **277,** 36793–36798
6. Ciechanover, A., and Brundin, P. (2003) *Neuron* **40,** 427–446
7. Hishikawa, N., Niwa, J., Doyu, M., Ito, T., Ishigaki, S., Hashizume, Y., and Sobue, G. (2003) *Am. J. Pathol.* **163,** 609–619
8. Mayer, R. J., Lowe, J., Lennox, G., Doherty, F., and Landon, M. (1989) *Prog. Clin. Biol. Res.* **317,** 809–818
9. Johnston, J. A., Ward, C. L., and Kopito, R. R. (1998) *J. Cell Biol.* **143,** 1883–1898
10. Kopito, R. R. (2000) *Trends Cell Biol.* **10,** 524–530
11. Kobayashi, T., Tanaka, K., Inoue, K., and Kakizuka, A. (2002) *J. Biol. Chem.* **277,** 47358–47365
12. Shimura, H., Hattori, N., Kubo, S., Mizuno, Y., Asakawa, S., Minoshima, S., Shimizu, N., Iwai, K., Chiba, T., Tanaka, K., and Suzuki, T. (2000) *Nat. Genet.* **25,** 302–305
13. Fukuchi, M., Imamura, T., Chiba, T., Ebisawa, T., Kawabata, M., Tanaka, K., and Miyazono, K. (2001) *Mol. Biol. Cell* **12,** 1431–1443
14. Ishigaki, S., Liang, Y., Yamamoto, M., Niwa, J., Ando, Y., Yoshihara, T., Takeuchi, H., Doyu, M., and Sobue, G. (2002) *J. Neurochem.* **82,** 576–584
15. Hirabayashi, M., Inoue, K., Tanaka, K., Nakadate, K., Ohsawa, Y., Kamei, Y., Popiel, A. H., Sinohara, A., Iwamatsu, A., Kimura, Y., Uchiyama, Y., Hori, S., and Kakizuka, A. (2001) *Cell Death Differ.* **8,** 977–984
16. Natsume, T., Yamauchi, Y., Nakayama, H., Shinkawa, T., Yanagida, M., Takahashi, N., and Isobe, T. (2002) *Anal. Chem.* **74,** 4725–4733
17. Matsuda, N., Suzuki, T., Tanaka, K., and Nakano, A. (2001) *J. Cell Sci.* **114,** 1949–1957
18. Bays, N. W., and Hampton, R. Y. (2002) *Curr. Biol.* **12,** R366–R371
19. Ye, Y., Meyer, H. H., and Rapoport, T. A. (2001) *Nature* **414,** 652–656
20. Braun, S., Matuschewski, K., Rape, M., Thoms, S., and Jentsch, S. (2002) *EMBO J.* **21,** 615–621
21. Jarosch, E., Taxis, C., Volkwein, C., Bordallo, J., Finley, D., Wolf, D. H., and Sommer, T. (2002) *Nat. Cell Biol.* **4,** 134–139
22. Rabinovich, E., Kerem, A., Frohlich, K. U., Diamant, N., and Bar-Nun, S. (2002) *Mol. Cell. Biol.* **23,** 626–634
23. Mizuno, Y., Hori, S., Kakizuka, A., and Okamoto, K. (2003) *Neurosci. Lett.* **343,** 77–80
24. Ito, T., Niwa, J., Hishikawa, N., Ishigaki, S., Doyu, M., and Sobue, G. (2003) *J. Biol. Chem.* **278,** 29106–29114
25. Meyer, H. H., Kondo, H., and Warren, G. (1998) *FEBS Lett.* **437,** 255–257
26. Kondo, H., Rabouille, C., Newman, R., Levine, T. P., Pappin, D., Freemont, P., and Warren, G. (1997) *Nature* **388,** 75–78
27. Rabouille, C., Kondo, H., Newman, R., Hui, N., Freemont, P., and Warren, G. (1998) *Cell* **92,** 603–610
28. Hetzer, M., Meyer, H. H., Walther, T. C., Bilbao-Cortes, D., Warren, G., and Mattaj, I. W. (2001) *Nat. Cell Biol.* **3,** 1086–1091
29. Frohlich, K. U., Fries, H. W., Rudiger, M., Erdmann, R., Botstein, D., and Mecke, D. (1991) *J. Cell Biol.* **114,** 443–453
30. Asai, T., Tomita, Y., Nakatsuka, S., Hoshida, Y., Myoui, A., Yoshikawa, H., and Aozasa, K. (2002) *Jpn. J. Cancer Res.* **93,** 296–304
31. Kawaguchi, Y., Okamoto, T., Taniwaki, M., Aizawa, M., Inoue, M., Katayama, S., Kawakami, H., Nakamura, S., Nishimura, M., Akiguchi, I., Kimura, J., Narumiya, S., and Kakizuka, A. (1994) *Nat. Genet.* **8,** 221–228
32. Matsumoto, M., Yada, M., Hatakeyama, S., Ishimoto, H., Tanimura, T., Tsuji, S., Kakizuka, A., Kitagawa, M., and Nakayama, K. I. (2004) *EMBO J.* **23,** 659–669
33. Watts, G. D., Wymer, J., Kovach, M. J., Mehta, S. G., Mumm, S., Darvish, D., Pestronk, A., Whyte, M. P., and Kimonis, V. E. (2004) *Nat. Genet.* **36,** 377–381
34. Koegl, M., Hoppe, T., Schlenker, S., Ulrich, H. D., Mayer, T. U., and Jentsch, S. (1999) *Cell* **96,** 635–644
35. Ghislain, M., Dohmen, R. J., Levy, F., and Varshavsky, A. (1996) *EMBO J.* **15,** 4884–4899
36. Meyer, H. H., Wang, Y., and Warren, G. (2002) *EMBO J.* **21,** 5645–5652
37. Nagahama, M., Suzuki, M., Hamada, Y., Hatsuzawa, K., Tani, K., Yamamoto, A., and Tagaya, M. (2003) *Mol. Biol. Cell* **14,** 262–273
38. Wojcik, C., Yano, M., and DeMartino, G. N. (2004) *J. Cell Sci.* **117,** 281–292
39. Dalal, S., and Hanson, P. I. (2001) *Cell* **104,** 5–8
40. Travers, K. J., Patil, C. K., Wodicka, L., Lockhart, D. J., Weissman, J. S., and Walter, P. (2000) *Cell* **101,** 249–258
41. Dai, R. M., and Li, C. C. (2001) *Nat. Cell Biol.* **3,** 740–744

# *Six1* controls patterning of the mouse otic vesicle

**Hidenori Ozaki[1], Kazuaki Nakamura[1], Jun-ichi Funahashi[2], Keiko Ikeda[1], Gen Yamada[3], Hisashi Tokano[4], Hiro-oki Okamura[4], Ken Kitamura[4], Shigeaki Muto[5], Hayato Kotaki[6], Katsuko Sudo[6], Reiko Horai[6], Yoichiro Iwakura[6] and Kiyoshi Kawakami[1,*]**

[1]Division of Biology, Center for Molecular Medicine, Jichi Medical School, Tochigi 329-0498, Japan
[2]Department of Molecular Neurobiology, Institute of Development, Aging and Cancer, Tohoku University, Sendai 980-8575, Japan
[3]Division of Transgenic Technology, Center for Animal Resources and Development, Kumamoto University, Kumamoto 860-0811, Japan
[4]Department of Otolaryngology, Tokyo Medical and Dental University, Tokyo 113-8519, Japan
[5]Division of Nephrology, Department of Internal Medicine, Jichi Medical School, Tochigi 329-0498, Japan
[6]Division of Cell Biology, Center for Experimental Medicine, Institute of Medical Science, University of Tokyo, Tokyo 108-8639, Japan
*Author for correspondence (e-mail: kkawakam@jichi.ac.jp)

*Accepted 24 October 2003*

Development 131, 551-562
Published by The Company of Biologists 2004
doi:10.1242/dev.00943

## Summary

***Six1* is a member of the Six family homeobox genes, which function as components of the Pax-Six-Eya-Dach gene network to control organ development. *Six1* is expressed in otic vesicles, nasal epithelia, branchial arches/pouches, nephrogenic cords, somites and a limited set of ganglia. In this study, we established *Six1*-deficient mice and found that development of the inner ear, nose, thymus, kidney and skeletal muscle was severely affected. *Six1*-deficient embryos were devoid of inner ear structures, including cochlea and vestibule, while their endolymphatic sac was enlarged. The inner ear anomaly began at around E10.5 and *Six1* was expressed in the ventral region of the otic vesicle in the wild-type embryos at this stage. In the otic vesicle of *Six1*-deficient embryos, expressions of *Otx1*, *Otx2*, *Lfng* and *Fgf3*, which were expressed ventrally in the wild-type otic vesicles, were abolished, while the expression domains of *Dlx5*, *Hmx3*, *Dach1* and *Dach2*, which were expressed dorsally in the wild-type otic vesicles, expanded ventrally. Our results indicate that *Six1* functions as a key regulator of otic vesicle patterning at early embryogenesis and controls the expression domains of downstream otic genes responsible for respective inner ear structures. In addition, cell proliferation was reduced and apoptotic cell death was enhanced in the ventral region of the otic vesicle, suggesting the involvement of *Six1* in cell proliferation and survival. In spite of the similarity of otic phenotypes of *Six1*- and *Shh*-deficient mice, expressions of *Six1* and *Shh* were mutually independent.**

Key words: *Six1*, Otic vesicle, Inner ear, Pattern formation, Cell proliferation, *Shh*, Mouse

## Introduction

The Six gene family was identified as a homologue of the *Drosophila sine oculis* (*so*) and is conserved in various species (Seo et al., 1999; Kawakami et al., 2000). Six gene products are characterized by the Six domain and Six-type homeodomain, which are required for specific DNA binding activity and function as transcription factors (Kawakami et al., 1996; Spitz et al., 1998; Ohto et al., 1999; Li et al., 2002; Lagutin et al., 2003). At present, six members of the family have been identified in mammals, and all members show a spatiotemporally regulated pattern of expression during embryogenesis, suggesting their involvement in embryonic development (Seo et al., 1999; Kawakami et al., 2000). The Six gene family is known to function as a component of the Pax-Six-Eya-Dach gene network. This property was originally identified in genetic studies using *Drosophila*. Compound eye formation has been extensively examined as a model system of organ development, and the important eye-forming genes, *eyeless* (*ey*, a *Pax6* homologue), *twin of eyeless* (*toy*, another *Pax6* homologue), *sine oculis* (*so*, a Six homologue), *eyes absent* (*eya*, an Eya homologue) and *dachshund* (*dac*, a Dach homologue), have been identified. Genetic and biochemical studies have revealed the hierarchy, cooperative relationships and physical interactions among these genes and their encoded proteins; *toy* activates *ey* (Czerny et al., 1999), and *ey* and/or *toy* activate *so* and *eya* (Halder et al., 1998; Niimi et al., 1999; Zimmerman et al., 2000), then *so* and *eya* cooperate to activate *dac* (Pignoni et al., 1997; Chen et al., 1997). In addition to such a hierarchy, reciprocal feedback loops operate to form complex regulatory gene networks (Chen et al., 1997; Pignoni et al., 1997). Of note is that the vertebrate homologues of these *Drosophila* genes, *Pax6* (Walther and Gruss, 1991), *Six3/Six6* (Oliver et al., 1995a; Toy et al., 1998), *Eya1/Eya2/Eya3* (Xu et al., 1997) and *Dach1/Dach2* (Caubit et al., 1999; Davis et al., 2001), are expressed in the developing eyes, and some of them were shown to be involved in eye development (Hill et al., 1991; Ton et al., 1991; Glaser et al., 1992; Oliver et al., 1996; Kobayashi et al., 1998; Loosli et al., 1999; Lagutin et al., 2001; Carl et al., 2002; Li et al., 2002; Lagutin et al., 2003). A similar gene network was found to control chick myogenesis, in which *Six1*, *Eya2* and *Dach2* synergistically regulate the expression of myogenic genes such as myogenin and *MyoD* (Heanue et

al., 1999). In addition, *Pax3* induces the expression of *Six1* and *Eya2* before induction of *MyoD* and myogenin expression (Ridgeway and Skerjanc, 2001). *Pax3* is involved in myogenesis also by activating *Dach2* expression and is reciprocally activated by *Dach2* (Heanue et al., 1999; Kardon et al., 2002). Furthermore, homologues of these gene families are expressed in various developing organs in a spatially and temporally overlapping manner during embryogenesis, suggesting that similar gene networks regulate the development of various organs in addition to the eye and skeletal muscles. In fact, an increasing number of loss-of-function mutations in Pax, Eya and Six genes have been reported to cause defects in various organs. *Pax2*-deficient mice show defects in eyes, ears and the urogenital system (Favor et al., 1996; Torres et al., 1996). Loss of *Eya1* in mice results in the absence or anomalies in the ear, thymus, parathyroid gland, kidney, thyroid and skeleton (Xu et al., 1999; Xu et al., 2002). For Six genes, inactivation of mouse *Six6* is associated with hypogenesis of the pituitary gland and retina (Li et al., 2002). *SIX3* mutations in humans cause holoprosencephaly, and *Six3* inactivation in mice results in a lack of anterior head structures, including eyes and nose (Wallis et al., 1999; Lagutin et al., 2003).

*Six1* is expressed in otic vesicles, nasal epithelia, branchial arches/pouches, nephrogenic cords, somites and a limited set of ganglia (Oliver et al., 1995b). However, it is unknown whether or how *Six1* is involved in the development of the inner ear, nose, branchial arch/pouch-derived organs, kidney, ganglia and skeletal muscles. To address this question, we generated and analyzed the organ development of *Six1*-deficient mice. The inner ear, nose, thymus, kidney and skeletal muscles are severely affected in *Six1*-deficient mice, suggesting crucial roles for *Six1* in the development of these organs. Among these phenotypes, the defects in inner ear development in the mutant mice are intriguing because inner ears develop elaborate structures with precise disposition and orientation in normal embryogenesis. They are derived from the otic vesicle by successive transformation and compartmentalization, but it is poorly understood how the patterning of the otic vesicle is established and what are the key factors for such complex processes. Thus, this paper focused on the analysis of inner ear development and identified the essential roles of *Six1* in otic vesicle patterning.

## Materials and methods

### Construction of the *Six1* targeting vector

The entire coding region of the murine *Six1* gene was isolated from a 129/SvJ mouse genomic library (Stratagene, La Jolla, California) using a *Six1* cDNA (Oliver et al., 1995b) as a probe, and the exon-intron organization was determined. An *Nco*I site was generated at the initiation codon by PCR mutagenesis to allow the insertion of an in-frame enhanced green fluorescent protein (EGFP) gene. The targeting vector was constructed in pBluescript KS(+) (Stratagene) and the organization is shown in Fig. 1A. In this construct the entire coding region, including exons 1 and 2, the intervening intron and the short stretch of the 3′ untranslated region of exon 2, were replaced with an EGFP fragment (*Nco*I-*Ssp*I, 1.0 kb) from pEGFP-N3 (Clontech, Palo Alto, California) and an *hph* cassette (*Eco*RV-*Pvu*II, 2 kb) from pPGK-*hph-bpA* (Horai et al., 1998). The diphtheria toxin A cassette (dt) (*Xho*I-*Not*I, 1.4 kb) from pMC1DTpA (Yagi et al., 1993) was added at the 3′ terminus for the negative selection. The resulting plasmid was linearized with *Sal*I at the 5′ end of the insert.

### ES cell screening and chimeric mouse production

The linearized targeting vector (80 μg) was electroporated (250 V, 500 μF) into $1 \times 10^7$ E14.1 ES cells (Kuhn et al., 1991) and transformants were selected with hygromycin B (230 μg/ml; Invitrogen Japan K.K., Tokyo) for 5-9 days. Homologous recombinants were screened by Southern blot hybridization. Genomic DNA from each resistant clone was digested with *Nco*I, analyzed by Southern blotting using the probes *Nco*I-*Sac*I, 1.2 kb fragment upstream of 5′ homology (5′ probe), and *Xba*I-*Eco*RI, 2.0 kb fragment downstream of 3′ homology (3′ probe), to confirm the correct homologous recombination at 5′ and 3′ sides, respectively (Fig. 1A). Chimeric mice were produced by the aggregation method (Horai et al., 1998). Male chimeras were bred with C57BL/6 female mice to check germline transmission. Heterozygous mice were intercrossed to produce *Six1*-deficient mice. Genotyping was carried out by Southern blot analysis (Fig. 1B) or PCR (data not shown) in combination with morphological analyses. In the PCR analysis, the targeted allele was detected with primers WtmSix1F (GCG CCC GGG CCC GTG CGC CCC) and KOmSix1R (TGC CCC AGG ATG TTG CCG TCC), and the wild-type allele with primers WtmSix1F and WtmSix1R (GCT TTC AGC CAC AGC TGC TGC).

In this study, *Shh* mutant mice with a targeted deletion of exon 2 of the gene were also used (Chiang et al., 1996) (kindly supplied by C. Chiang and C. C. Hui).

Mice were kept under specific pathogen-free conditions in environmentally controlled clean rooms at the Center for Experimental Medicine, Jichi Medical School, and at the Laboratory Animal Research Center, Institute of Medical Science, University of Tokyo. All mice used in this study were sacrificed by cervical translocation or anesthetization with diethyl ether. The experiments were conducted according to the institutional ethical guidelines for animal experiments and safety guidelines for gene manipulation experiments.

### Histological examinations

Embryos and neonates were fixed in 10% formalin or 4% PFA in PBS, embedded in paraffin wax and then cut into 5-μm thick serial sections. De-waxed sections were stained with hematoxylin and eosin as described previously (Ozaki et al., 2001). Alcian Blue/Alizarin Red staining of neonatal skeletons was performed as described previously (Wallin et al., 1994).

### RNA in situ hybridization

In situ hybridization was performed using digoxygenin (DIG)-labeled antisense riboprobes as described previously (Xu and Wilkinson, 1998). *Eya1* riboprobe was synthesized from a 528 bp *Hind*III fragment of pHM6Eya1 (Ohto et al., 1999) subcloned into pBluescript KS(+). *Six4* riboprobe was synthesized from a 630 bp *Pst*I fragment (ntd 1545-2175 of *Six4* SM type cDNA) subcloned into pBluescript KS(+). The following cDNAs were also used for in situ hybridization probes: *Six1* (Oliver et al., 1995b), *Otx1* and *Otx2* (Matsuo et al., 1995), *Fgf3* (Wilkinson et al., 1988), *Lfng* (Morsli et al., 1998), *Dlx5* (Miyama et al., 1999), *Dach1* (Caubit et al., 1999), *Dach2* (Davis et al., 2001), *Pax2* (Nishinakamura et al., 2001), *Bmp4* (a kind gift from N. Ueno), *Hmx3* (Wang et al., 1998), *Shh* (Urase et al., 1996), *Ptch* (Goodrich et al., 1996), *Gli1* (Hui et al., 1994), *Wnt2b* (Riccomagno et al., 2002).

### TUNEL analysis

For terminal deoxynucleotidyl transferase-mediated dUDP nick-end labeling (TUNEL), embryos were fixed in 4% PFA in PBS, embedded in OCT compound, and frozen and sectioned into serial cryosections. Apoptotic cells were detected with the In Situ Cell Death Detection Kit, POD (Roche Diagnostics Mannheim, Germany). Briefly,

fragmented DNA in apoptotic cells was end-labeled with fluorescein and the labeled DNA was detected with anti-fluorescein antibody conjugated with peroxidase and a chromogenic substrate.

### BrdU incorporation

Pregnant female mice of gestation day 10.5 and 11.5 were intraperitoneally injected with 100 mg 5-bromo-2′-deoxyuridine (BrdU) per kg body weight. Embryos were collected 1.5 hours later and processed for preparation of 8-μm thick paraffin sections as described above. De-waxed serial sections crossing otic vesicles were treated with 2 N HCl/0.5% Triton X-100 in PBS for 30 minutes at room temperature and rinsed with 0.1 M borate buffer (pH 8.5), followed by incubation in 0.6% $H_2O_2$ in PBS for 30 minutes at room temperature. Subsequently, the sections were incubated overnight in peroxidase-labeled anti-BrdU (Roche) at 4°C. After washing, sections were stained in 0.4 mg/ml diaminobenzidine, 0.68 mg/ml imidazole, 0.01% $H_2O_2$, and 50 mM Tris-HCl (pH 7.4).

### Paint-fill analysis

Paint-fill was performed as described previously (Bissonnette and Fekete, 1996). In brief, embryos were fixed in Bodian's fixative, dehydrated through graded ethanol solutions, then cleared in methyl salicylate and injected into the lumen of the membranous labyrinth with white paint diluted 1 to 100 in methyl salicylate.

### ABR threshold measurements

The auditory evoked response was recorded with stainless steel needle electrodes inserted subcutaneously into the vertex (active), left and right of the retro-auricular regions (inactive) and the opposite thigh (ground). The stimulus sound in peak equivalent sound pressure level (peSPL) of a tone pips of 0.1 millisecond slopes, 1 millisecond duration, 70 millisecond repeat interval with 5.6, 8.0, 12.0, 18.0, 24.0, 32.0 kHz frequencies was given by free field in an electrically shielded room. A tweeter (PT-R111, Pioneer) was placed 10 cm in front of the external acoustic foramen. The stimulus sound pressure was corrected by a Bruel & Kjaer-type 2636 noise meter. A microcomputer (ER-2104, GE Marquet) was used to analyze the response. Auditory thresholds were obtained for each stimulus by varying at 10 dB steps up and down to identify the lowest level at which an auditory brain response (ABR) pattern could be recognized. These experiments were conducted in five wild-type and six heterozygous mice at 5 to 6 weeks of age.

## Results

### Generation of *Six1*-deficient mice

To explore the developmental roles of *Six1*, we inactivated *Six1* in ES cells by replacing the entire coding region with EGFP gene (Fig. 1A). Two independent ES clones were confirmed as homologous recombinants (data not shown), and both of them gave germline chimeric mice. These chimeric mice were crossed with C57BL/6 to obtain F1 heterozygous mutant mice. Heterozygotes appeared normal in appearance and grew up to adulthood as wild type (data not shown). The concentrations of $Na^+$, $K^+$, $Cl^-$, $Ca^{2+}$, $Mg^{2+}$, inorganic phosphate, urea nitrogen, creatinine, albumin and uric acid in serum and urine were measured with an auto-analyzer, and we observed no significant difference in the concentrations of all these parameters between the wild-type and heterozygous mutant mice (data not shown). We also performed ABR testing for hearing impairment in the heterozygous mutant mice. The ABR thresholds were 25.0±5.3, 14.0±5.2, 14.0±5.2, 11.0±3.2, 10.0±0.0 and 14.0±5.2 dBpeSPL for the wild-type mice and 23.3±4.9, 15.0±5.2, 10.8±2.9, 10.0±0.0, 10.8±2.9 and 14.2±5.1 dBpeSPL for the heterozygotes at frequencies of 5.6, 8.0, 12.0, 18.0, 24.0 and 32.0 kHz, respectively, and there were no significant differences in these values between the wild-type and heterozygous mutant mice.

Homozygous mutants were born at Mendelian frequency and showed few body movements but were apnoeic and died immediately after birth. They had micrognathia, and the eyelids were sometimes open (data not shown). No *Six1* mRNA was detected in homozygotes (Fig. 1C), confirming that the entire coding region of *Six1* was replaced by EGFP gene in this mutant. In the following analyses, we used neonates and embryos from F1 heterozygous matings.

### Defects in ears, nose, thymus, kidneys and skeletal muscles of *Six1*-deficient neonates

Dissection analyses and hematoxylin and eosin (H-E) staining of sections of the neonates revealed defects in the ears, nose, thymus, kidneys and skeletal muscles in

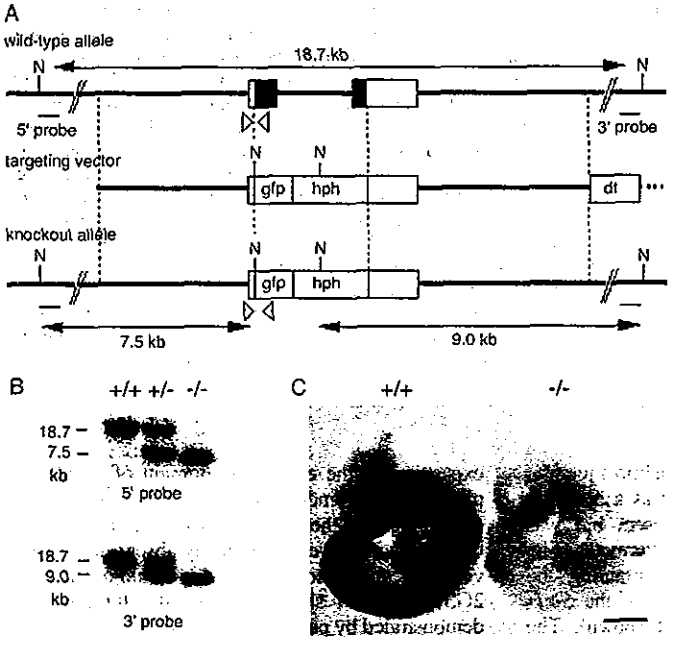


**Fig. 1.** Generation of *Six1*-deficient mice. (A) Targeting strategy of *Six1*. The *Six1* gene consists of two exons (indicated by boxes), and the coding regions are marked in black. The entire coding regions were replaced with the EGFP gene (gfp) and the *hygromycin-B-phosphotransferase* gene (hph). Open arrowheads indicate the positions of PCR primers for genotyping. (B) Southern blot analyses of wild-type (+/+), heterozygous (+/–), and homozygous (–/–) mutant neonates. Tail DNA was digested with *Nco*I and hybridized to 5′ probe (upper panel) and 3′ probe (lower panel). The size of each band is indicated on the left side. (C) In situ hybridization to *Six1* in E10.5 wild-type and homozygous embryos. Absence of *Six1* mRNA was confirmed in the *Six1*-deficient embryo. dt, diphtheria toxin A gene; N, *Nco*I site. Scale bar: 1 mm.


**Fig. 2.** Defects in the inner and middle ear in *Six1*-deficient mice. (A,B) Transverse sections at the level of the pinna of the neonates. The semicircular canals and the endolymphatic sac are irregularly formed in the *Six1*$^{-/-}$ neonates. The semicircular canals and the common crus are fused, forming a large cavity (B, arrowhead). (C-F) *Wnt2b* expression analysis by in situ hybridization. Expansion of the *Wnt2b* expression domain in the *Six1*$^{-/-}$ embryos (E,F) compared with wild type (C,D) indicates that the enlarged region is the endolymphatic sac at E17.5 (E) and endolymphatic duct at E11.5 (F). In F, *Wnt2b* was expressed in the medial half of the otic vesicle, which corresponds to the enlarged endolymphatic duct as depicted in L (otic vesicle shown in F was flattened during the hybridization process). (G,H) Transverse sections at the cochlea level show complete loss of the cochlea in *Six1*$^{-/-}$ neonates (asterisk). (I,J) Alcian blue/Alizarin red staining of neonatal skeletons revealed malformations of ossicles. (K,L) Transverse sections of wild-type (K) and *Six1*$^{-/-}$ (L) embryos at E11.5. The cochlear region does not extend ventrally and the endolymphatic duct is dilated in *Six1*$^{-/-}$ embryos. (M-P) Transverse sections of wild-type (M,O) and *Six1*$^{-/-}$ (N,P) embryos at E12.5. The endolymphatic duct and canal plate are formed, but the morphology is abnormal in the *Six1*$^{-/-}$ embryo (N). The cochlea is completely absent in *Six1*$^{-/-}$ embryos (P, asterisks). (Q-T) Lateral views of the paint-filled inner ear of wild-type (Q) and *Six1*$^{-/-}$ (R) E18.5 embryos and otic vesicles of wild-type (S) and *Six1*$^{-/-}$ (T) E10.5 embryos. (R′) Posterior view of the same inner ear as (R). Relative positions are aligned between wild type and *Six1*$^{-/-}$. The two ventrally protruding structures observed in (R and R′) are the ventral ends of residual cavities of the canal plate-like structure and the endolymphatic duct. More than five *Six1*$^{-/-}$ neonates or embryos at each stage were analyzed, and virtually the same results were obtained. co, cochlea; cp, canal plate; cpl, canal plate-like structure; d, dorsal; ed, endolymphatic duct; es, endolymphatic sac; in, incus; la, lateral; m, medial; ma, malleus; mc, Meckel's cartilage; ov, otic vesicle; sc, semicircular canals; st, stapes; tr, tympanic ring. Scale bars: 100 μm.

the *Six1*-deficient mice. In the inner ear, the dorsalmost parts of semicircular canals and common crus remained as a common fused space. The endolymphatic sac was present but was irregularly larger in size than that of wild-type littermates (Fig. 2A,B) The enlargement was confirmed by comparing the diameter of the paint-filled endolymphatic sacs of the *Six1*-deficient and the wild-type embryos (data not shown). The expansion of the expression domain of *Wnt2b*, an expression marker for the endolymphatic sac and duct, also supports the enlargement of the endolymphatic sac (Fig. 2C,E). Other parts of the inner ear were completely absent, including the cochlea, vestibule and accompanying vestibulo-acoustic ganglia (Fig. 2G,H, data not shown). These structural defects were also demonstrated by paint-fill analyses (Fig. 2Q,R,R′). Because *Six1*

expression was evident in the branchial arch and periotic mesenchymes (Fig. 1C, Fig. 4C), we examined the middle ear defects in the *Six1*-deficient neonates and found malformations of the malleus and the incus and the absence of the stapes (Fig. 2I,J). In the nose, *Six1*-deficient mice manifested a hollowed nasal region with traces of nasal bleeding (data not shown). A pair of mere simple, rounded nostrils was present with no nasal epithelium, by contrast to the well-branched cavities with thick layers of nasal epithelia in the wild-type littermates (Fig. 3A,B). Both nasal cavities did not connect with the oral cavity or the nasopharynx, and the vomeronasal organs were absent in *Six1*-deficient mice (data not shown). The surrounding ossified region was abnormally enlarged (Fig. 3B), as observed in the inner ear (Fig. 2B,H). *Six1*-deficient mice also lacked a thymus (Fig. 3C,D). Kidneys were severely affected to variable degrees (Fig. 3E,F). Small kidneys with normal structure were found in mild cases (data not shown), while both kidneys were absent in extreme cases, although the ureters were always formed but were occasionally shorter (Fig. 3F). We also found markedly reduced skeletal muscle mass of the trunk, limbs, diaphragm and tongue (Fig. 3G,H, data not shown). The thymus, kidney, ear, nose and skeletal muscle defects are consistent with the *Six1*-deficient mice with different targeting strategy (Laclef et al., 2003a; Laclef et al., 2003b; Xu et al., 2003). These affected organs correlated well with the expression sites of *Six1* during development, such as otic vesicles, nasal pits, branchial arches/pouches, nephrogenic cords and somites (Oliver et al., 1995b). These results indicate that *Six1* is required for the formation of the ear, nose, thymus, kidneys and skeletal muscles.

### Defects in inner ear appear at mid-gestation in *Six1*-deficient embryos

To determine the developmental stages at which the inner ear defects start to appear, *Six1*-deficient mice of several embryonic stages were sectioned and analyzed by H-E staining. At E9.5, otic vesicles were morphologically normal in *Six1*-deficient embryos, but the vestibulo-acoustic ganglia were missing (data not shown). At E10.5 and E11.5, the otic vesicles began to compartmentalize into saccular and utricular regions. The saccular region extended to the ventral side as a thin bulge in the wild type (Fig. 2K). By contrast, the extension of the saccular region to the ventral side did not occur in *Six1*-deficient embryos (Fig. 2L). The endolymphatic duct was observed as a thin outpocketing from the medial side of the otic vesicle in wild-type embryos, while the endolymphatic duct was observed as a large swelling in *Six1*-deficient embryos (Fig. 2K,L). The thin outpocketing and the large swelling region coincided with the expression domain of *Wnt2b* (Fig. 2D,F). We also used paint-fill analyses to compare otic vesicle structures at E10.5 with those of the wild type and confirmed the absence of the thin outpocketing and the dilatation of the endolymphatic duct in *Six1*-deficient otic vesicles (Fig. 2S,T, data not shown). At E12.5, the main structures of the inner ear (cochlea, saccule, utricle, endolymphatic duct and canal plates, from which three semicircular canals and common crus are formed) were distinguishable in the wild type (Fig. 2M,O, data not shown). By contrast, the dorsal extremity of the semicircular canals and common crus was observed as a fused cavity, and abnormally large endolymphatic duct was present (Fig. 2N), while other parts were completely absent in *Six1*-deficient embryos (Fig. 2P, data not shown).

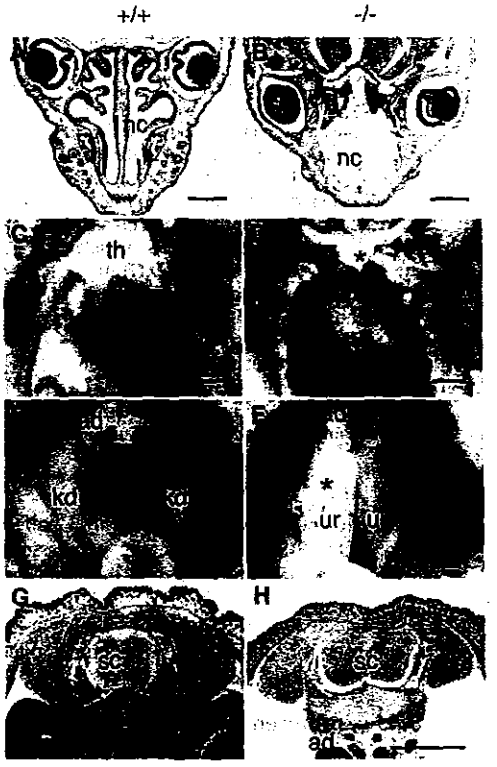


**Fig. 3.** Defects in the formation of the nose, thymus, kidney and skeletal muscles. Histological analyses of the wild-type (A,C,E,G) and the *Six1*$^{-/-}$ (B,D,F,H) neonates. (A,B) Transverse sections of the nasal region. Nasal cavities form complex, branched structures with nasal epithelia in the wild type (A), and a pair of simple round cavities with no nasal epithelia is seen in the *Six1*$^{-/-}$ neonates (B). (C,D) The thymus is prominent anterior to the heart in the wild type (C) but completely absent in the *Six1*$^{-/-}$ neonate (D, asterisk). (E,F) Kidney defects in *Six1*$^{-/-}$ mice. Note the bilateral renal aplasia (F, asterisks). (G,H) Abdominal transverse sections. Note severe reduction of skeletal muscle mass in *Six1*$^{-/-}$ neonates (H). More than five pairs of wild-type and *Six1*$^{-/-}$ neonates were analyzed and virtually the same results obtained except for the kidney (see text). ad, adrenal gland; kd, kidney; nc, nasal cavity; sc, spinal cord; th, thymus; ur, ureter. Scale bars: 1 mm.

In summary, the development of the inner ear was defective at mid-gestation around E10.5-12.5.

### Expression of *Six1* in the developing inner ear

To gain insight into the function of *Six1* during inner ear development, we first examined the expression pattern of *Six1* by in situ hybridization in the wild type (Fig. 4A-F) and GFP fluorescence in heterozygous embryos (Fig. 4G-I). *Six1* mRNA was first detected in the otic placode and the surrounding surface ectoderm at E8.5 (Fig. 4A). *Six1* expression became prominent at the invaginating otic pit and the nascent otic vesicle at E9.5 (Fig. 4B,C), consistent with previous observations (Oliver et al., 1995b). Notably, the expression level was considerably lower in the dorsalmost region than in the other region of the otic vesicle (Fig. 4C). At E10.5, *Six1*

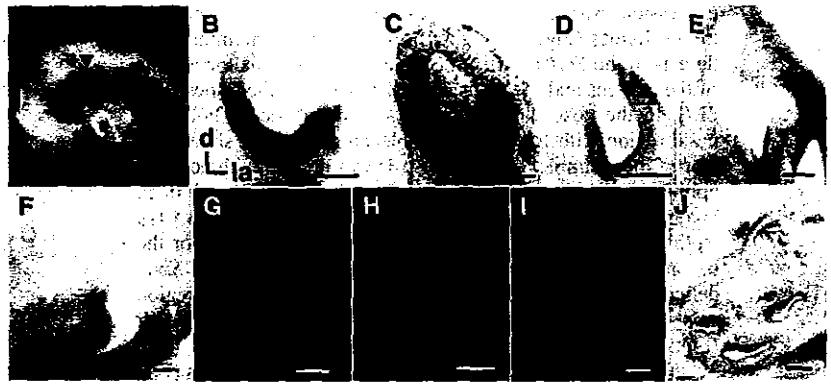


Fig. 4. *Six1* expression pattern during inner ear development detected by in situ hybridization in the wild type (A-F) and by GFP luminescence in the heterozygotes (G-I) viewed laterally (A) and in transverse sections (B-I). (A) At E8.5, *Six1* is weakly expressed in the otic placode (arrowhead) and the surrounding surface ectoderm. (B) At E9.5, *Six1* is expressed in the invaginating otic pit and (C) in the whole region of the otic vesicle except the dorsalmost region. (D,G) At E10.5, *Six1* is expressed in the ventral half of the otic vesicle. (E) At E11.5 and (F,H) E12.5, *Six1* is expressed exclusively in the cochlea. (I) Expression of *Six1* in the cochlea is maintained at E14.5 embryos. (J) A bright field image of the section in (I) stained with hematoxylin and eosin. More than three embryos at each stage were analyzed and virtually the same results obtained. d, dorsal; la, lateral. Scale bars: 100 μm.

expression was limited to the ventral half of the otic vesicle (Fig. 4D,G). Subsequently, the expression domain of *Six1* became gradually restricted to the cochlear region at E11.5 (Fig. 4E) and E12.5 (Fig. 4F,H). At later stages, *Six1* transcripts were detected exclusively in the cochlea at E14.5 (Fig. 4I), and the expression of *Six1* in the cochlear duct persisted in the neonate (data not shown).

### *Six1* is required for correct patterning of the otic vesicle

The morphological defects in *Six1*-deficient mice were not restricted to the cochlea but extended to all regions of the inner ear except the dorsal extremity of the semicircular canals (Fig. 2). The missing ventral structures of the mutant mouse inner ear appeared to be related to the expression domain of *Six1* in the ventral otic vesicle at E9.5-10.5 (Fig. 4C,D). The absence of cochlea and vestibule and the enlargement of the endolymphatic sac prompted us to examine the following three possibilities: that the specification along the dorsoventral axis within the otic vesicle is altered in *Six1*-deficient embryos, that the cells within the ventral region of the *Six1*-deficient otic vesicle undergo enhanced apoptotic cell death, and that the cells within the ventral region of the *Six1*-deficient otic vesicle proliferate at a lower rate than those of the wild type. We assessed the first possibility by comparing the expression pattern of genes differentially expressed within the otic vesicle at E9.5-10.5. The ventralmost cells of the otic vesicle are marked by the co-expression of *Otx1* and *Otx2* (Morsli et al., 1999). *Otx1* and *Otx2* were not expressed in the *Six1*-deficient otic vesicle, by contrast to the wild type, although an ectopic faint expression of *Otx1* was reproducibly detected in the dorsalmost region (Fig. 5A-D). *Lunatic Fringe* (*Lfng*), a component of the Notch signaling pathway, is known as a molecular marker for inner ear sensory structures (Morsli et al., 1998). *Lfng* was expressed in the rostroventral region in the wild type (Fig. 5E), but no such expression was noted in the *Six1*-deficient otic vesicle (Fig. 5F). *Fgf3*, which is required for normal morphogenesis of the inner ear (Mansour et al., 1993), was expressed in the rostroventral region of the wild-type otic vesicle as *Lfng* (Fig. 5G), while the expression of *Fgf3* was absent in the *Six1*-deficient otic vesicle (Fig. 5H). *Bmp4* is an early marker for the superior, lateral and posterior cristae. It was expressed in the restricted regions of the otic vesicle in the wild type (Fig. 5I), but no such expression was noted in *Six1*-deficient mice (Fig. 5J).

The dorsal side of the otic vesicle gives rise to the semicircular canals and endolymphatic duct/sac and is well marked by the expression of *Dlx5*, which is required for the normal development of the semicircular canals and endolymphatic duct/sac (Fig. 5K) (Acampora et al., 1999; Depew et al., 1999). In *Six1*-deficient embryos, the expression domain of *Dlx5* expanded to the entire otic vesicle (Fig. 5L). The expression domains of *Hmx2* and *Hmx3*, both of which are required for the formation of the vestibular structures (Wang et al., 1998; Wang et al., 2001), expanded ventrally from the dorsolateral side in the *Six1*-deficient otic vesicle (Fig. 5M,N, data not shown). *Dach1* is a member of the Dach family genes, which constitute the Pax-Six-Eya-Dach gene network. It was also expressed at the dorsal edge of the otic vesicle in the wild-type embryos (Fig. 5O). *Dach1* expression expanded ventrally along the medial and lateral sides almost down to the ventral end in *Six1*-deficient embryos (Fig. 5P). *Dach2*, another member of Dach family genes, was expressed mainly in the dorsal end of the otic vesicle in wild-type embryos, but *Dach2* expression domain was expanded ventrally along the lateral side of the otic vesicles (Fig. 5Q,R).

We also examined the expression pattern of *Pax2*, *Eya1* and *Six4* to clarify whether the expression of these genes is dependent on *Six1*. These genes are components of the Pax-Six-Eya-Dach gene network and are co-expressed in the otic vesicle. *Pax2* was expressed in the medial side of the otic vesicle of the wild-type and *Six1*-deficient embryos (Fig. 5S,T). *Eya1* expression in the ventral side of the wild-type otic vesicle was maintained in the *Six1*-deficient otic vesicle (Fig. 5U,V). *Six4* was expressed in the ventral side of the otic vesicle in wild-type embryos, and this expression pattern was almost the same in the *Six1*-deficient embryo (Fig. 5W,X). However, the most abundantly expressed regions of *Eya1* and *Six4* appeared slightly shifted from the ventromedial (wild-type) to the ventrolateral (*Six1*-deficient) side of the otic vesicle. These results suggest that the expression of *Pax2*, *Eya1* and *Six4* in the otic vesicle is not dependent on *Six1*.

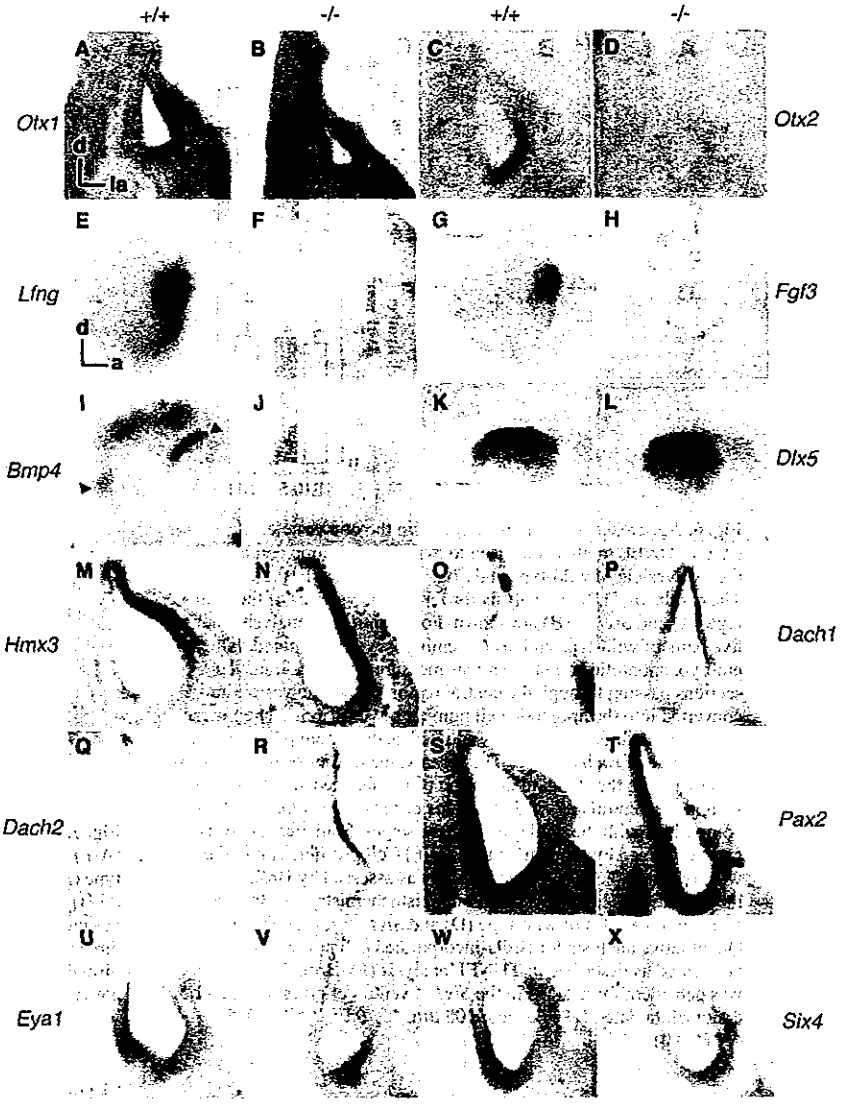


**Fig. 5.** *Six1* specifies the expression domains of differentially expressed genes in the otic vesicle. Transverse section or whole-mount view of the otic vesicle of in situ hybridized wild type (A,C,E,G,I,K,M,O,Q,S,U,W) and *Six1*$^{-/-}$ embryos (B,D,F,H,J,L,N,P,R,T,V,X) of E10.5 (A-J,M-X) and E9.5 (K,L). (A,B) No *Otx1* expression in the *Six1*$^{-/-}$ otic vesicle except for ectopic faint expression at the dorsal end. (C,D) Absence of *Otx2* transcripts in the *Six1*$^{-/-}$ otic vesicle. (E,F) *Lfng* is expressed in the rostroventral region of the otic vesicle in the wild-type embryo but not in the *Six1*$^{-/-}$ embryo. (G,H) *Fgf3* expression in the rostroventral region of the otic vesicle in the wild type is lost in the *Six1*$^{-/-}$ embryo. (I,J) *Bmp4* expression in the wild-type otic vesicle (arrowheads) is lost in the *Six1*$^{-/-}$ otic vesicle. Staining in the ectoderm over the dorsal region of the otic vesicle (asterisk) has also disappeared. (K,L) *Dlx5* is expressed dorsally in the wild type but in the whole region of the otic vesicle in the *Six1*$^{-/-}$ embryo. (M,N) *Hmx3* expression domain is located only in the dorsolateral region in the wild type but is expanded ventrally in the *Six1*$^{-/-}$ embryo. (O,P) *Dach1* expression is restricted to the dorsalmost region in the wild type, but the expression domain extends ventrally in the *Six1*$^{-/-}$ otic vesicle. Signals in the neighboring mesenchyme are also observed in the lower right side of the otic vesicle. (Q,R) *Dach2* is expressed at the dorsal end of the otic vesicle in the wild type, but the expression domain of *Dach2* is expanded ventrally along the lateral side in *Six1*$^{-/-}$. (S,T) *Pax2* is expressed in medial and ventral sides of the otic vesicle of both wild-type and *Six1*$^{-/-}$ embryos. (U,V) *Eya1* is expressed in the ventral side of the wild-type and the *Six1*$^{-/-}$ otic vesicle. (W,X) *Six4* expression in the ventral side of the otic vesicle is maintained in the *Six1*$^{-/-}$ embryo. More than three pairs of wild-type and *Six1*$^{-/-}$ embryos were analyzed and virtually the same results obtained. A-D and M-X: top, dorsal side (d); right, lateral side (la). E-L: top, dorsal side (d); right, anterior side (a).

In conclusion, loss of *Six1* expression leads to marked changes in the expression domains of many genes in the otic vesicle, suggesting that the first possibility listed above is the case: i.e. the specification along the dorsoventral axis within the otic vesicle is altered in *Six1*-deficient embryos. Next, we assessed the second and third possibilities by TUNEL method and BrdU incorporation.

## Enhanced apoptosis and reduced cell proliferation in the ventral otic vesicle

We examined whether enhanced apoptotic cell death or reduced cell proliferation within the ventral region of the otic vesicle contributes to the inner ear phenotype. TUNEL method was used to detect apoptotic cells in the otic vesicle at E10.5 and E11.5, just before the extensive morphological changes. Several apoptotic cells were detected in the wild type, while enhanced apoptotic cell death was observed in the ventral and medial sides of the otic vesicles of *Six1*-deficient embryos at E11.5 (Fig. 6A,B). Statistical analysis revealed significant augmentation of apoptosis at E10.5 and E11.5 (Fig. 6C). We also examined BrdU incorporation in the otic vesicle at the same developmental stages. In the wild type and in the *Six1*-deficient embryos at E11.5, BrdU incorporation was abundant in the ventral region of the otic vesicle (Fig. 6D). By contrast,

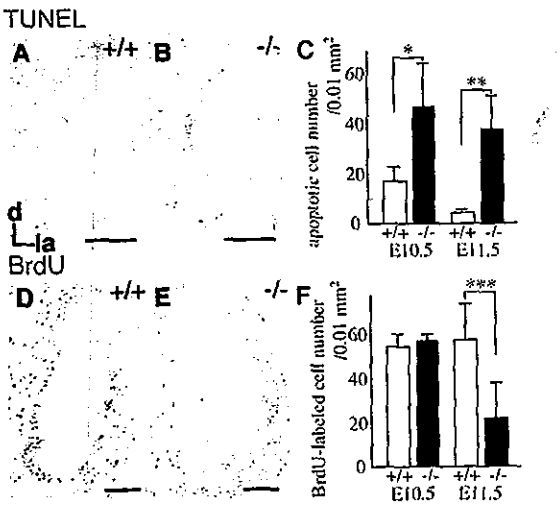


Fig. 6. Apoptosis and cell proliferation in the otic vesicle. (A-C) TUNEL method was used to examine apoptotic cell death in the otic vesicle of wild-type and *Six1*$^{-/-}$ embryos at E10.5 and E11.5. The results of TUNEL analysis for E11.5 otic vesicles of the wild type (A) and *Six1*$^{-/-}$ (B) are shown. For quantitative analysis, four to five pairs of wild-type and *Six1*$^{-/-}$ embryos were examined. For each embryo, apoptotic cell number was measured on three transverse sections passing through the central region of the otic vesicle and converted into the apoptotic cell number per 0.01 mm$^2$. Their mean value for the three sections was adopted as the datum point for the otic vesicle of each embryo. The mean value of four or five embryos is shown with the standard deviation (C). Enhanced apoptosis was seen in the ventral and medial regions of the *Six1*$^{-/-}$ otic vesicle in comparison with the wild type in these stages. Statistical analysis was performed by Student's *t*-test. (D-F) Cell proliferation in the wild-type and the *Six1*$^{-/-}$ otic vesicle was assessed by BrdU incorporation. The results of immunohistochemistry for BrdU at E11.5 otic vesicles of wild-type (D) and *Six1*$^{-/-}$ (E) are shown. Quantitative analysis for BrdU-incorporated cell number was performed as described in TUNEL analysis (F). BrdU incorporation was considerably reduced in the *Six1*$^{-/-}$ ventral otic vesicle at E11.5. d, dorsal; la, lateral. Scale bars: 100 μm. *$P$<0.05; **$P$<0.005; ***$P$<0.01.

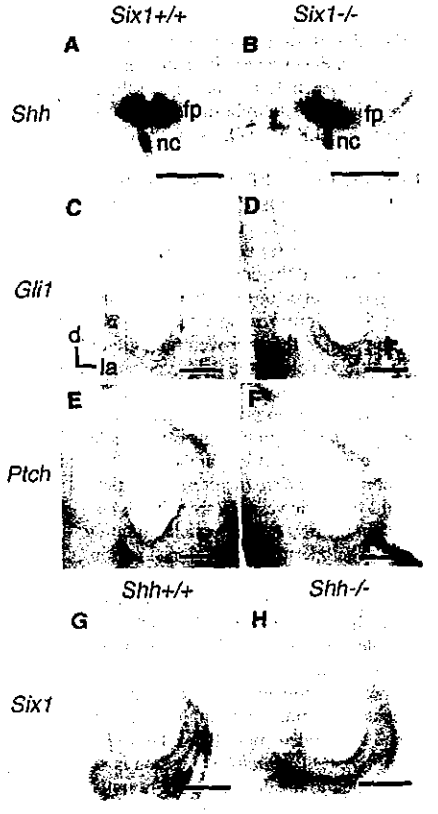


Fig. 7. Expression patterns of *Shh*, *Gli1*, *Ptch* and *Six1*. (A-F) Expressions of *Shh* (A,B), *Gli1* (C,D) and *Ptch* (E,F) in wild-type (A,C,E) and *Six1*$^{-/-}$ (B,D,F) embryos at E10.5. (G,H) Expression of *Six1* in wild-type (G) and *Shh*$^{-/-}$ (H) otic vesicles at E10.5. Three pairs of wild-type and *Six1*$^{-/-}$ embryos and three pairs of wild-type and *Shh*$^{-/-}$ embryos were analyzed and virtually the same results obtained. d, dorsal; la, lateral. fp, floor plate; nc, notochord. Scale bars: 100 μm.

the incorporation was profoundly reduced in the ventral side of the otic vesicles of *Six1*-deficient embryos at E11.5 (Fig. 6E). A significant decrease in the number of BrdU-incorporated cells was observed at E11.5 but not at E10.5 (Fig. 6F). The reduced cell proliferation observed in *Six1*-deficient otic vesicles may be in line with the roles of *Six1* in cell cycle control (Ford et al., 1998). These results suggest that the lack of ventral structures of the inner ear in the *Six1*-deficient mice is partly due to enhanced apoptosis and reduced cell proliferation, as well as altered patterning of the otic vesicle.

### Sonic hedgehog (Shh) signaling pathway is independent of *Six1*

We noticed that the inner ear phenotype of *Six1*-deficient mice is similar to that of *Shh*-deficient mice, which is characterized by the absence of the cochlear duct and vestibulocochlear ganglia, ventral expansion of the expression domains of *Dlx5*, loss of the expression domain of *Otx2*, and ventral restriction of *Otx1* expression (Riccomagno et al., 2002). The similarity of the phenotypes could be explained by the assumption that the Shh signaling pathway is dependent on *Six1* expression or vice versa. To test this possibility, we first examined the expression of *Shh* and the Shh-inducible genes, *Ptch* and *Gli1* in *Six1*-deficient embryos. *Shh* was expressed in the notochord and the floor plate near the otic vesicles in the wild type (Fig. 7A), and this expression pattern was virtually unchanged in *Six1*-deficient embryos (Fig. 7B). *Ptch* and *Gli1* were expressed in the otic vesicle and periotic mesenchyme in the wild-type embryo, and these expression patterns were similar in *Six1*-deficient embryos (Fig. 7C-F). Next, we examined *Six1* expression in *Shh*-deficient embryos (Chiang et al., 1996). *Six1* expression was abundant in the ventral region of the otic vesicles in *Shh*-deficient embryos, as observed in the wild type (Fig. 7G,H). These results indicate that the Shh signaling pathway is independent of *Six1* and that the expression of *Six1* in the otic vesicle is also independent of the Shh signaling pathway.

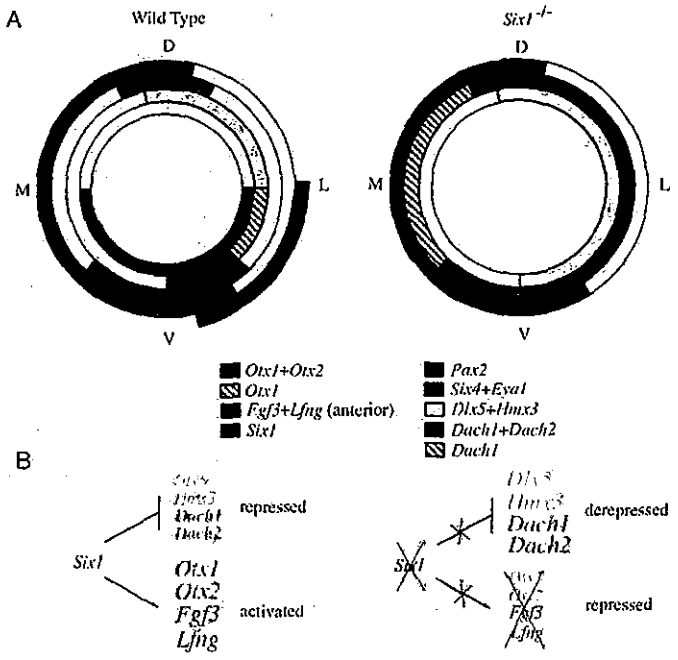


**Fig. 8.** (A) Schematic representation of expression of genes in otic vesicles of the wild-type (left) and *Six1*$^{-/-}$ mice (right) at E10.5. In the otic vesicle of the wild-type, otic genes are expressed in the specified regions represented in different colors. In the wild-type otic vesicle, *Six1* is expressed in the ventral half of the otic vesicle. In the otic vesicle of *Six1*$^{-/-}$, the expression domains of *Dlx5*, *Hmx3*, *Dach1* and *Dach2* are expanded ventrally, and the expressions of the ventral marker genes (*Otx1*, *Otx2*, *Fgf3* and *Lfng*) are lacking due to the absence of *Six1*. (B) Regulation of gene expression by *Six1* in the ventral otic vesicle. *Six1* activates the expression of ventral marker genes, *Otx1*, *Otx2*, *Lfng* and *Fgf3*, but represses dorsal marker genes, *Dlx5*, *Hmx3*, *Dach1* and *Dach2*, and contributes to the patterning of the otic vesicle. D, dorsal; L, lateral; M, medial; V, ventral.

## Discussion

### Establishment of otic vesicle patterning by *Six1*

The inner ear originates from a transient embryonic structure, the otic vesicle. Successive transformations and compartmentalization of the otic vesicle give rise to the entire membranous region of inner ear structures. The fate of cells in the otic vesicle is dependent on the gene expression specific to each compartment of the otic vesicle (Fekete, 1999). For example, *Dlx5*, which is expressed in the dorsal side of the otic vesicle, is required for the formation of the semicircular canals (Acampora et al., 1999; Depew et al., 1999). *Otx1*, which is expressed in the ventral side, is needed for the correct morphogenesis of the cochlea (Acampora et al., 1996). The establishment of such a gene expression profile in the otic vesicle, orchestrated by networks or cascades of transcription factors, is essential for inner ear development. However, the genes involved in these networks and components of the cascades are largely unknown. Our study showed for the first time that *Six1* functions to establish the correct expression pattern of many otic genes and contributes to the formation of the majority of inner ear structures. Altered expression pattern of many otic genes (Fig. 5) results in the loss of specifications of the ventral region of the otic vesicle, with resultant expansion of the dorsally specified domains at E9.5-10.5, and consequently in the absence of the cochlea and most of the vestibule, together with dysgenesis of residual region of semicircular canals and enlargement of the endolymphatic sac in *Six1*-deficient neonates (Fig. 2). The ventral expression of *Six1* in the otic vesicle at E9.5-10.5 suggests that *Six1* activates the expression of *Otx1*, *Otx2*, *Lfng* and *Fgf3* and represses the expression of *Dlx5*, *Hmx3*, *Dach1* and *Dach2* (Fig. 8). Although it is unknown whether these genes are regulated directly by *Six1*, it is concluded that *Six1* plays a key role in establishing otic vesicle patterning.

In addition to the patterning of the otic vesicle along the dorsoventral axis, *Six1* may play roles in the otic vesicle patterning along the anteroposterior and/or mediolateral axes, because anteroposteriorly and/or mediolaterally asymmetrical expression patterns of *Otx1*, *Otx2*, *Lfng*, *Fgf3* and *Bmp4* were also affected (Fig. 5). For these issues, further histological examinations and analyses of molecular marker expression will be required.

Furthermore, our results showed a marked reduction of cell proliferation and enhanced apoptosis in the ventral otic vesicle in *Six1*-deficient embryos (Fig. 6). This may contribute to the inner ear phenotype lacking most of the ventral structures. Thus, *Six1* controls inner ear development by regulating cell death and proliferation as well as by establishing otic vesicle patterning.

### Phenotypic similarity of the inner ear compared with *Shh*-deficient mice

Previous and present studies indicated that specification of the cochlea is dependent on Shh signaling and that perturbation of otic vesicle pattering in *Shh*-deficient mice (Riccomagno et al., 2002) is similar to that of *Six1*-deficient mice. Considering these phenotypic similarities of inner ear formation between *Six1*- and *Shh*-deficient mice, we assumed a genetic interaction between *Six1* and *Shh*. However, the expression patterns of *Shh*, *Gli1* and *Ptch* in *Six1*-deficient mice and that of *Six1* in *Shh*-deficient mice (Chiang et al., 1996) indicate that the expressions of *Shh*, *Gli1* and *Ptch* are not dependent on *Six1*, and that the expression of *Six1* is not dependent on the Shh signaling pathway in and around the otic vesicle at E10.5 (Fig. 7). Another possible mode of genetic interaction is through functional cooperation between Six1 and the components of Shh signaling cascades. Shh protein is emanated from the notochord and/or the floor plate, probably giving a gradient of Shh across the otic vesicle with a high concentration in the ventral side and a low concentration in the dorsal side. This Shh gradient would enhance putative collaborative interaction between downstream components of Shh signaling cascades and Six1 in the ventral otic vesicle. Modulation of the transactivating function of Six1 by Shh signaling would be one of the plausible mechanisms. However, we cannot exclude

independent actions of Six1 and components of Shh signaling cascades in the otic vesicle. For example, expression of *Pax2* in the medialventral otic vesicle is maintained in *Six1*-deficient mice (Fig. 5S,T), but is downregulated in *Shh*-deficient mice (Riccomagno et al., 2002). To determine whether *Six1* and *Shh* interact genetically, it would be important to examine the phenotypes of the *Six1/Shh* double mutant.

### Roles of *Six1* in Pax-Six-Eya-Dach gene network

Six genes function as components of the Pax-Six-Eya-Dach gene network in organ development. In the ventral otic vesicle, *Six1* is co-expressed with *Pax2*, *Pax8*, *Six4* and *Eya1* to control inner ear development. Outside the otic vesicles, various combinations of Pax, Six, Eya and Dach genes are co-expressed in the primordia of the organs affected in *Six1*-deficient mice: the olfactory placode (*Pax6*, *Six1*, *Six2*, *Six3*, *Six4*, *Six6*, *Eya1*, *Eya2*, *Eya4*); the thymus (*Pax9*, *Six1*, *Six4*, *Eya1*); the metanephros (*Pax2*, *Pax8*, *Six1*, *Six2*, *Six4*, *Eya1*); and the somite/myotome (*Pax3*, *Six1*, *Six4*, *Eya1*, *Eya2*, *Eya4*, *Dach1*). *Six1* plays important roles in the development of these organs, probably through the control of patterning and/or cell proliferation, as observed in the otic vesicle. Notably, Dach genes are not co-expressed with Six and Eya genes in the ventral otic vesicle, nose or kidney (Figs 4, 5, data not shown). Furthermore, Dach expression domains were expanded ventrally in the *Six1*-deficient otic vesicle, indicating that *Six1* represses the expression of Dach genes in the ventral otic vesicle. Likewise, augmentation of Dach expression was observed in the nasal pit of *Six1*-deficient embryos (data not shown), indicating that expression of the Dach gene is repressed by *Six1* also in the nasal pit. These findings are in contrast to *Drosophila* compound eye formation and chick myogenesis. In both those cases, Pax, Six and Eya are co-expressed with Dach, cooperatively to execute the developmental programs. Thus, the Pax-Six-Eya gene network lacking Dach may demarcate the two placode-derived sensory organs, the inner ear and the nose, and the kidney from other organs such as the eye and the skeletal muscles. In addition, hierarchy among Pax, Six, Eya and Dach genes in the otic vesicle has been revealed in this study. That is, the expression patterns and levels of *Eya1* and *Pax2* were not affected but expression domains of *Dach1* and *Dach2* were expanded ventrally in the *Six1*-deficient otic vesicle (Fig. 5). Conversely, *Six1* expression is lost but *Pax2* expression is not disturbed in the *Eya1*-deficient otic vesicle (Xu et al., 1999). Thus, in the otic vesicle, expression of *Eya1* and *Pax2* is independent of *Six1*, expression of *Six1* depends on *Eya1*, and *Six1* controls *Dach1* and *Dach2* expression. In the myotome, *Six4* expression is not dependent on *Six1*, as observed in the otic vesicle (Laclef et al., 2003a), but *Pax2* expression is dependent on *Six1* in metanephric mesenchyme (Xu et al., 2003). The similarities among these organ primordia in the context of the Pax-Six-Eya(-Dach) network and the diversity in selecting members from respective gene hierarchies among them raise interesting issues regarding the ontogeny of these organs during evolution.

In conclusion, our study identified the essential role of *Six1* in the regulation of otic vesicle patterning. Together with mice homozygous for other Pax, Six, Eya and Dach genes, *Six1*-deficient mice should allow a comprehensive understanding of the roles of the Pax-Six-Eya-Dach gene network in various organogeneses.

We thank Chin Chiang for providing *Shh*-deficient mice; Yoko Watanabe, Miwa Nakamura and Sachiko Nozawa for technical assistance; Makoto Yamakado, Kuniko Shimazaki and Heide Ford for technical advice; and Makoto Kobayashi and Shigeru Sato for critical reading of the manuscript. We thank Shinichi Aizawa, David Wilkinson, Douglas Epstein, Takashi Momoi, Jun Motoyama, Doris K. Wu, Ryuichi Nishinakamura, Hiroshi Shibuya, Akira Murakami, Naoto Ueno, Stefan Krauss, Graeme Mardon, Peter Gruss and Thomas Lufkin for the plasmids for probes used in this work. We also thank Pascal Maire for sharing the information about *Six1* gene organization. This work was supported by grants from the Ministry of Education, Culture, Sports, Science and Technology of Japan and from the Ministry of Health, Labour and Welfare of Japan.

## References

**Acampora, D., Mazan, S., Avantaggiato, V., Barone, P., Tuorto, F., Lallemand, Y., Brulet, P. and Simeone, A.** (1996). Epilepsy and brain abnormalities in mice lacking the Otx1 gene. *Nat. Genet.* **14**, 218-222.

**Acampora, D., Merlo, G. R., Paleari, L., Zerega, B., Postiglione, M. P., Mantero, S., Bober, E., Barbieri, O., Simeone, A. and Levi, G.** (1999). Craniofacial, vestibular and bone defects in mice lacking the Distal-less-related gene *Dlx5*. *Development* **126**, 3795-3809.

**Bissonnette, J. P. and Fekete, D. M.** (1996). Standard atlas of the gross anatomy of the developing inner ear of the chicken. *J. Comp. Neurol.* **368**, 620-630.

**Carl, M., Loosli, F. and Wittbrodt, J.** (2002). Six3 inactivation reveals its essential role for the formation and patterning of the vertebrate eye. *Development* **129**, 4057-4063.

**Caubit, X., Thangarajah, R., Theil, T., Wirth, J., Nothwang, H.-G., Ruther, U. and Krauss, S.** (1999). Mouse Dac, a novel nuclear factor with homology to *Drosophila dachshund* shows a dynamic expression in the neural crest, the eye, the neocortex, and the limb bud. *Dev. Dyn.* **214**, 66-80.

**Chen, R., Amoui, M., Zhang, Z. and Mardon, G.** (1997). Dachshund and eyes absent proteins form a complex and function synergistically to induce ectopic eye development in Drosophila. *Cell* **91**, 893-903.

**Chiang, C., Litingtung, Y., Lee, E., Young, K. E., Corden, J. L., Westphal, H. and Beachy, P. A.** (1996). Cyclopia and defective axial patterning in mice lacking Sonic hedgehog gene function. *Nature* **383**, 407-413.

**Czerny, T., Halder, G., Kloter, U., Souabni, A., Gehring, W. J. and Busslinger, M.** (1999). Twin of eyeless, a second Pax-6 gene of Drosophila, acts upstream of eyeless in the control of eye development. *Mol. Cell* **3**, 297-307.

**Davis, R. J., Shen, W., Sandler, Y. I., Heanue, T. A. and Mardon, G.** (2001). Characterization of mouse Dach2, a homologue of Drosophila dachshund. *Mech. Dev.* **102**, 169-179.

**Depew, M. J., Liu, J. K., Long, J. E., Presley, R., Meneses, J. J., Pedersen, R. A. and Rubenstein, J. L.** (1999). Dlx5 regulates regional development of the branchial arches and sensory capsules. *Development* **126**, 3831-3846.

**Favor, J., Sandulache, R., Neuhauser-Klaus, A., Pretsch, W., Chatterjee, B., Senft, E., Wurst, W., Blanquet, V., Grimes, P., Sporle, R. et al.** (1996). The mouse Pax2$^{1Neu}$ mutation is identical to a human PAX2 mutation in a family with renal-coloboma syndrome and results in developmental defects of the brain, ear, eye, and kidney. *Proc. Natl. Acad. Sci. USA* **93**, 13870-13875.

**Fekete, D. M.** (1999). Development of the vertebrate ear: insights from knockouts and mutants. *Trends Neurosci.* **22**, 263-269.

**Ford, H. L., Kabingu, E. N., Bump, E. A., Mutter, G. L. and Pardee, A. B.** (1998). Abrogation of the $G_2$ cell cycle checkpoint associated with overexpression of HSIX1: a possible mechanism of breast carcinogenesis. *Proc. Natl. Acad. Sci. USA* **95**, 12608-12613.

**Glaser, T., Walton, D. S. and Maas, R. L.** (1992). Genomic structure, evolutionary conservation and aniridia mutations in the human PAX6 gene. *Nat. Genet.* **2**, 232-239.

**Goodrich, L. V., Johnson, R. L., Milenkovic, L., McMahon, J. A. and Scott, M. P.** (1996) Conservation of the hedgehog/patched signaling pathway from flies to mice: induction of a mouse patched gene by Hedgehog. *Genes Dev.* **10**, 301-312.

**Halder, G., Callaerts, P., Flister, S., Walldorf, U., Kloter, U. and Gehring, W. J.** (1998). Eyeless initiates the expression of both sine oculis and eyes

absent during Drosophila compound eye development. *Development* **125**, 2181-2191.

**Heanue, T. A., Reshef, R., Davis, R. J., Mardon, G., Oliver, G., Tomarev, S., Lassar, A. B. and Tabin, C. J.** (1999). Synergistic regulation of vertebrate muscle development by Dach2, Eya2, and Six1, homologs of genes required for Drosophila eye formation. *Genes Dev.* **13**, 3231-3243.

**Hill, R. E., Favor, J., Hogan, B. L., Ton, C. C., Saunders, G. F., Hanson, I. M., Prosser, J., Jordan, T., Hastie, N. D. and van Heyningen, V.** (1991). Mouse small eye results from mutations in a paired-like homeobox-containing gene. *Nature* **354**, 522-525.

**Horai, R., Asano, M., Sudo, K., Kanuka, H., Suzuki, M., Nishihara, M., Takahashi, M. and Iwakura, Y.** (1998). Production of mice deficient in genes for interleukin (IL)-1α, IL-1β, IL-1α/β, and IL-1 receptor antagonist shows that IL-1β is crucial in turpentine-induced fever development and glucocorticoid secretion. *J. Exp. Med.* **187**, 1463-1475.

**Hui, C. C., Slusarski, D., Platt, K. A., Holmgren, R. and Joyner, A. L.** (1994). Expression of three mouse homologs of the Drosophila segment polarity gene cubitus interruptus, Gli, Gli-2, and Gli-3, in ectoderm- and mesoderm-derived tissues suggests multiple roles during postimplantation development. *Dev. Biol.* **162**, 402-413.

**Kardon, G., Heanue, T. A. and Tabin, C. J.** (2002). Pax3 and Dach2 positive regulation in the developing somite. *Dev. Dyn.* **224**, 350-355.

**Kawakami, K., Ohto, H., Ikeda, K. and Roeder, R. G.** (1996). Structure, function and expression of a murine homeobox protein AREC3, a homologue of Drosophila sine oculis gene product, and implication in development. *Nucleic Acids Res.* **24**, 303-310.

**Kawakami, K., Sato, S., Ozaki, H. and Ikeda, K.** (2000). Six family genes-structure and function as transcription factors and their roles in development. *Bioessays* **22**, 616-626.

**Kobayashi, M., Toyama, R., Takeda, H., Dawid, I. B. and Kawakami, K.** (1998). Overexpression of the forebrain-specific homeobox gene six3 induces rostral forebrain enlargement in zebrafish. *Development* **125**, 2973-2982.

**Kuhn, R., Rajewsky, K. and Muller, W.** (1991). Generation and analysis of interleukin-4 deficient mice. *Science* **254**, 707-710.

**Laclef, C., Hamard, G., Demignon, J., Souil, E., Houbron, C. and Maire, P.** (2003a). Altered myogenesis in Six1-deficient mice. *Development* **130**, 2239-2252.

**Laclef, C., Souil, E., Demignon, J. and Maire, P.** (2003b). Thymus, kidney and craniofacial abnormalities in Six1 deficient mice. *Mech. Dev.* **120**, 669-679.

**Lagutin, O., Zhu, C. C., Furuta, Y., Rowitch, D. H., McMahon, A. P. and Oliver, G.** (2001). Six3 promotes the formation of ectopic optic vesicle-like structures in mouse embryos. *Dev. Dyn.* **221**, 342-349.

**Lagutin, O. V., Zhu, C. C., Kobayashi, D., Topczewski, J., Shimamura, K., Puelles, L., Russell, H. R., McKinnon, P. J., Solnica-Krezel, L. and Oliver, G.** (2003). Six3 repression of Wnt signaling in the anterior neuroectoderm is essential for vertebrate forebrain development. *Genes Dev.* **17**, 368-379.

**Li, X., Perissi, V., Liu, F., Rose, D. W. and Rosenfeld, M. G.** (2002). Tissue-specific regulation of retinal and pituitary precursor cell proliferation. *Science* **297**, 1180-1183.

**Loosli, F., Winkler, S. and Wittbrodt, J.** (1999). Six3 overexpression initiates the formation of ectopic retina. *Genes Dev.* **13**, 649-654.

**Mansour, S. L., Goddard, J. M. and Capecchi, M. R.** (1993). Mice homozygous for a targeted disruption of the proto-oncogene int-2 have developmental defects in the tail and inner ear. *Development* **117**, 13-28.

**Matsuo, I., Kuratani, S., Kimura, C., Takeda, N. and Aizawa, S.** (1995). Mouse Otx2 functions in the formation and patterning of rostral head. *Genes Dev.* **9**, 2646-2658.

**Miyama, K., Yamada, G., Yamamoto, T. S., Takagi, C., Miyado, K., Sakai, M., Ueno, N. and Shibuya, H.** (1999). A BMP-inducible gene, Dlx5, regulates osteoblast differentiation and mesoderm induction. *Dev. Biol.* **208**, 123-133.

**Morsli, H., Choo, D., Ryan, A., Johnson, R. and Wu, D. K.** (1998). Development of the mouse inner ear and origin of its sensory organs. *J. Neurosci.* **18**, 3327-3335.

**Morsli, H., Tuorto, F., Choo, D., Postiglione, M. P., Simeone, A. and Wu, D. K.** (1999). Otx1 and Otx2 activities are required for the normal development of the mouse inner ear. *Development* **126**, 2335-2343.

**Niimi, T., Seimiya, M., Kloter, U., Flister, S. and Gehring, W. J.** (1999). Direct regulatory interaction of the eyeless protein with an eye-specific enhancer in the sine oculis gene during eye induction in Drosophila. *Development* **126**, 2253-2260.

**Nishinakamura, R., Matsumoto, Y., Nakao, K., Nakamura, K., Sato, A., Copeland, N. G., Gilbert, D. J., Jenkins, N. A., Scully, S., Lacey, D. L. et al.** (2001) Murine homolog of SALL1 is essential for ureteric bud invasion in kidney development. *Development* **128**, 3105-3115.

**Ohto, H., Kamada, S., Tago, K., Tominaga, S. I., Ozaki, H., Sato, S. and Kawakami, K.** (1999). Cooperation of Six and Eya in activation of their target genes through nuclear translocation of Eya. *Mol. Cell. Biol.* **19**, 6815-6824.

**Oliver, G., Mailhos, A., Wehr, R., Copeland, N. G., Jenkins, N. A. and Gruss, P.** (1995a). Six3, a murine homologue of the sine oculis gene, demarcates the most anterior border of the developing neural plate and is expressed during eye development. *Development* **121**, 4045-4055.

**Oliver, G., Wehr, R., Jenkins, N. A., Copeland, N. G., Cheyette, B. N. R., Hartenstein, V., Zipursky, S. L. and Gruss, P.** (1995b). Homeobox genes and connective tissue patterning. *Development* **121**, 693-705.

**Oliver, G., Loosli, F., Koster, R., Wittbrodt, J. and Gruss, P.** (1996). Ectopic lens induction in fish in response to the murine homeobox gene Six3. *Mech. Dev.* **60**, 233-239.

**Ozaki, H., Watanabe, Y., Takahashi, K., Kitamura, K., Tanaka, A., Urase, K., Momoi, T., Sudo, K., Sakagami, J., Asano, M. et al.** (2001). Six4, a putative myogenin gene regulator, is not essential for mouse embryonal development. *Mol. Cell. Biol.* **21**, 3343-3350.

**Pignoni, F., Hu, B., Zavitz, K. H., Xiao, J., Garrity, P. A. and Zipursky, S. L.** (1997). The eye-specification proteins So and Eya form a complex and regulate multiple steps in Drosophila eye development. *Cell* **91**, 881-891.

**Riccomagno, M. M., Martinu, L., Mulheisen, M., Wu, D. K. and Epstein, D. J.** (2002). Specification of the mammalian cochlea is dependent on Sonic hedgehog. *Genes Dev.* **16**, 2365-2378.

**Ridgeway, A. G. and Skerjanc, I. S.** (2001). Pax3 is essential for skeletal myogenesis and the expression of Six1 and Eya2. *J. Biol. Chem.* **276**, 19033-19039.

**Seo, H. C., Curtiss, J., Mlodzik, M. and Fjose, A.** (1999). Six class homeobox genes in Drosophila belong to three distinct families and are involved in head development. *Mech. Dev.* **83**, 127-139.

**Spitz, F., Demignon, J., Porteu, A., Kahn, A., Concordet, J. P., Daegelen, D. and Maire, P.** (1998). Expression of myogenin during embryogenesis is controlled by Six/sine oculis homeoproteins through a conserved MEF3 binding site. *Proc. Natl. Acad. Sci. USA* **95**, 14220-14225.

**Ton, C. C., Hirvonen, H., Miwa, H., Weil, M. M., Monaghan, P., Jordan, T., van Heyningen, V., Hastie, N. D., Meijers-Heijboer, H., Drechsler, M. et al.** (1991). Positional cloning and characterization of a paired box- and homeobox-containing gene from the aniridia region. *Cell* **67**, 1059-1074.

**Torres, M., Gomez-Pardo, E. and Gruss, P.** (1996). Pax2 contributes to inner ear patterning and optic nerve trajectory. *Development* **122**, 3381-3391.

**Toy, J., Yang, J. M., Leppert, G. S. and Sundin, O. H.** (1998). The Optx2 homeobox gene is expressed in early precursors of the eye and activates retina-specific genes. *Proc. Natl. Acad. Sci. USA* **95**, 10643-10648.

**Urase, K., Mukasa, T., Igarashi, H., Ishii, Y., Yasugi, S., Momoi, M. Y. and Momoi, T.** (1996). Spatial expression of Sonic hedgehog in the lung epithelium during branching morphogenesis. *Biochem. Biophys. Res. Commun.* **225**, 161-166.

**Wallin, J., Wilting, J., Koseki, H., Fritsch, R., Christ, B. and Balling, R.** (1994). The role of Pax-1 in axial skeleton development. *Development* **120**, 1109-1121.

**Wallis, D. E., Roessler, E., Hehr, U., Nanni, L., Wiltshire, T., Richieri-Costa, A., Gillessen-Kaesbach, G., Zackai, E. H., Rommens, J. and Muenke, M.** (1999). Mutations in the homeodomain of the human SIX3 gene cause holoprosencephaly. *Nat. Genet.* **22**, 196-198.

**Walther, C. and Gruss, P.** (1991). Pax-6, a murine paired box gene, is expressed in the developing CNS. *Development* **113**, 1435-1449.

**Wang, W., Van De Water, T. and Lufkin, T.** (1998). Inner ear and maternal reproductive defects in mice lacking the Hmx3 homeobox gene. *Development* **125**, 621-634.

**Wang, W., Chan, E. K., Baron, S., Van De Water, T. and Lufkin, T.** (2001). Hmx2 homeobox gene control of murine vestibular morphogenesis. *Development* **128**, 5017-5029.

**Wilkinson, D. G., Peters, G., Dickson, C. and McMahon, A. P.** (1988) Expression of the FGF-related proto-oncogene int-2 during gastrulation and neurulation in the mouse. *EMBO J.* **7**, 691-695.

**Xu, P.-X., Woo, I., Her, H., Beier, D. R. and Maas, R. L.** (1997). Mouse Eya homologues of the Drosophila eyes absent gene require Pax6 for expression in lens and nasal placode. *Development* **124**, 219-231.

**Xu, P.-X., Adams, J., Peters, H., Brown, M. C., Heaney, S. and Maas, R.**

(1999). Eya1-deficient mice lack ears and kidneys and show abnormal apoptosis of organ primordia. *Nat. Genet.* **23**, 113-117.

**Xu, P.-X., Zheng, W., Laclef, C., Maire, P., Maas, R. L., Peters, H. and Xu, X.** (2002). Eya1 is required for the morphogenesis of mammalian thymus, parathyroid and thyroid. *Development* **129**, 3033-3044.

**Xu, P.-X., Zheng, W., Huang, L., Maire, P., Laclef, C. and Silvius, D.** (2003). Six1 is required for the early organogenesis of mammalian kidney. *Development* **130**, 3085-3094.

**Xu, Q. and Wilkinson, D. G.** (1998). In situ hybridization of mRNA with hapten labelled probes. In *In Situ Hybridization: a Practical Approach* (ed. D. G. Wilkinson), pp. 87-106. London: Oxford University Press.

**Yagi, T., Nada, S., Watanabe, N., Tamemoto, H., Kohmura, N., Ikawa, Y. and Aizawa, S.** (1993). A novel negative selection for homologous recombinants using diphtheria toxin A fragment gene. *Anal. Biochem.* **214**, 77-86.

**Zimmerman, J. E., Bui, Q. T., Liu, H. and Bonini, N. M.** (2000). Molecular genetic analysis of Drosophila eyes absent mutants reveals an eye enhancer element. *Genetics* **154**, 237-246.

0013-7227/04/$15.00/0
*Printed in U.S.A.*

Endocrinology 145(11):5044–5048

doi: 10.1210/en.2004-0054

# *Interleukin (IL)-6*, But Not *IL-1*, Induction in the Brain Downstream of Cyclooxygenase-2 Is Essential for the Induction of Febrile Response against Peripheral IL-1$\alpha$

KYOKO KAGIWADA, DAI CHIDA, TOMOYA SAKATANI, MASAHIDE ASANO, AYA NAMBU, SHIGERU KAKUTA, AND YOICHIRO IWAKURA

*Division of Cell Biology, Center for Experimental Medicine, Institute of Medical Science, University of Tokyo, Tokyo 108-8639, Japan*

**IL-1 is an endogenous pyrogen produced upon inflammation or infection. Previously, we showed that, upon injection with turpentine, IL-1 is induced in the brain in association with the development of fever. The role of endogenous IL-1 in the brain and the signaling cascade to activate thermosensitive neurons, however, remain to be elucidated. In this report, febrile response was analyzed after peripheral injection of IL-1$\alpha$. We found that a normal febrile response was induced even in *IL-1$\alpha$/$\beta$*-deficient mice, indicating that production of IL-1 in the brain is not necessarily required for the response. In contrast, *IL-6*-deficient mice did not exhibit a febrile response. *Cyclooxygenase (Cox)-2* expression in the brain was strongly induced 1.5 h after injection of IL-1$\alpha$, whereas *IL-6* expression was observed 3 h after the injection. *Cox-2* expression in the brain was not influenced by *IL-6* deficiency, whereas indomethacin, an inhibitor of cyclooxygenases, completely inhibited induction of *IL-6*. These observations suggest a mechanism of IL-1-induced febrile response in which IL-1 in the blood activates *Cox-2*, with the resulting prostaglandin $E_2$ inducing *IL-6* in the brain, leading to the development of fever. (*Endocrinology* 145: 5044–5048, 2004)**

IL-1 IS A MAJOR mediator of inflammation, performing numerous functions related to host defense mechanisms by regulating not only the immune system but also the neuronal and endocrine systems (1). Two molecular species, IL-1$\alpha$ and IL-1$\beta$, are known as agonists and an antagonist, IL-1 receptor antagonist (IL-1Ra), which binds to the same receptors, is also known. Two IL-1 receptors, the type I IL-1 receptor (IL-1RI) and type II (IL-1RII), exist; only the former transduces IL-1 signaling and the latter rather acts as a decoy. IL-1 is produced by a large variety of cells, including monocytes and macrophages, and IL-1Rs are expressed on a wide range of cells in the immune, neural, and endocrine systems. Because IL-1Rs are induced upon peripheral inflammation in the brain, particularly the hypothalamus, hippocampus, and choroid plexus (2–4), a role for IL-1 has been suggested in the neuronal system.

Fever is a common response of the body to various stresses such as infection and inflammation. Such peripheral stimuli are transmitted to the brain through the nervous system and also by "endogenous pyrogens" (5). Although it is well known that circulating cytokines such as IL-1 and tumor necrosis factor (TNF)$\alpha$ are important endogenous pyrogens, the precise mechanism by which these cytokines induce fever through activation of the thermoregulatory neurons in the hypothalamus remains to be elucidated. It is especially interesting to elucidate how these cytokines stimulate relevant thermoregulatory brain structures, because these large hydrophilic polypeptides hardly penetrate the blood-brain barrier (BBB) (6, 7).

We showed previously that IL-1 expression was induced in the diencephalon of the brain upon injection with turpentine, and that the febrile response to turpentine was abolished in IL-1$\alpha$/$\beta$-deficient mice, suggesting involvement of IL-1 in the brain in the development of fever (8). Consistently, IL-1RI-deficient mice also failed to respond to turpentine (9). On the other hand, it has been demonstrated that endogenous hypothalamic IL-1$\beta$ is not necessary for the development of IL-1$\alpha$-, IL-1$\beta$- or lipopolysaccharide (LPS)-induced fever (10). It is not known, however, whether or not a febrile response can be induced in the complete absence of both IL-1$\alpha$ and IL-1$\beta$ in the brain.

It is known that prostaglandin (PG)$E_2$ is involved in the development of fever during inflammation, because inhibitors of cyclooxygenases, which catalyze synthesis of $PGH_2$, a precursor of $PGE_2$, can suppress febrile response (11), and mice lacking the $EP_3$ receptor, one of the receptors for $PGE_2$, showed an impaired febrile response during the first hour after IL-1$\beta$ injection (12). Although two types of cyclooxygenases (Cox) are known, it was suggested that only Cox-2 is involved in the febrile response upon inflammation (8, 13–15). Furthermore, endogenously induced IL-6 has also been suggested to be involved in the febrile response induced by IL-1 (16). However, the relationship among IL-1, IL-6, and Cox-2 in the brain has not been established conclusively.

In this report, to elucidate the roles of IL-1, which is endogenously induced in the brain during fever, we examined the febrile response in *IL-1$\alpha$/$\beta$*-deficient mice upon peripheral administration of IL-1$\alpha$. Furthermore, we analyze the

Abbreviations: BBB, Blood-brain barrier; BW, body weight; Cox, cyclooxygenase; IL-1R, IL-1 receptor; IL-1Ra, IL-1R antagonist; LPS, lipopolysaccharide; PG, prostaglandin.

*Endocrinology* is published monthly by The Endocrine Society (http://www.endo-society.org), the foremost professional society serving the endocrine community.

signaling cascade in the brain using *IL-1α/β*- and *IL-6*-deficient mice.

## Materials and Methods

### *Reagents*

Recombinant murine IL-1α was obtained from Pepro Tech EC LTD (London, UK). The lyophilized protein was dissolved in pyrogen-free 0.9% NaCl (saline) containing 0.1% BSA (A9306; Sigma, St. Louis, MO). Indomethacin was obtained from Sigma.

### *Animals*

*IL-1α/β*-doubly deficient mice were produced as described (8), and *IL-6*-deficient mice were kindly provided by Dr. Manfred Kopf (17). These mice were backcrossed to C57BL/6J mice for eight generations, and C57BL/6J mice were used as controls. Mice were housed individually from weaning at 4 wk of age, and sex- and age-matched adult (9–15 wk of age) male mice were used for each experiment. Mice were kept under specific, pathogen-free conditions in an environmentally controlled clean room at the Center for Experimental Medicine, Institute of Medical Science, University of Tokyo. They were housed at an ambient temperature of 24 C and a daily cycle of 12-h light/dark (0800–2000 h light). All experiments were carried out both according to the institutional ethical guidelines for animal experiments and the safety guidelines for gene manipulation experiments.

### *Measurement of body temperature*

Intraperitoneal temperature of mice was measured using an electric thermometer and tips (ELAMS system; BioMedic Data System, Inc., Maywood, NJ) with an accuracy of 0.1 C. All the tips were tested and adjusted before use. Mice were anesthetized with Nembutal, and the tip was implanted chronically into their peritoneal cavity and ligated to the peritoneum. The position of the tips was verified by postmortem examination. These mice were used for experiments 18 d after the thermometer implantation. IL-1α [1 μg/kg body weight (BW)] was injected iv at 1100 h, and the temperature was measured every 15 min by a person who was accustomed to using the system.

### *Northern blot hybridization analysis*

Northern blot hybridization was performed as described previously using mouse *IL-1α*, *IL-1β*, Cox-2, IL-6, and *β-actin* cDNA as probes (8). Wild-type, *IL-1α/β*-deficient, and *IL-6*-deficient mice were injected with IL-1α (1 μg/kg BW). Mice were killed 1.5 and 3 h after injection, and poly-$A^+$ RNA was isolated from the diencephalons. Samples from four mice were pooled for each genotype. Poly-$A^+$ RNA (8–11 μg) was electrophoresed on a denatured agarose gel and hybridized with specific probes; β-actin was used as a control. Relative radioactivities of the *IL-1α*, *IL-1β*, IL-6, and *Cox-2* bands were compared after normalization with the intensity of the *β-actin* band.

### *Indomethacin treatment*

Mice were injected with indomethacin (10 mg/kg BW, ip injection) dissolved in a buffer containing 0.9% NaCl, 5% ethanol, and 4% sodium hydrogen carbonate, or the buffer only 30 min before IL-1 (1 μg/kg BW, iv) injection or saline injection, and *IL-6* and *Cox-2* mRNA levels were measured 3 h after the treatment by Northern blot hybridization.

### *Statistical analysis*

Averages ± SD are shown. In Fig. 1, Student's *t* test was used to evaluate statistical significance. Animals with consecutive missing temperature recordings, due to failure of the telemetry system, were excluded from the statistical analysis. In Fig. 2, Student's paired *t* test was performed to compare before (basal) and after (1.5 h or 3 h after IL-1 injection) data for each genotype.

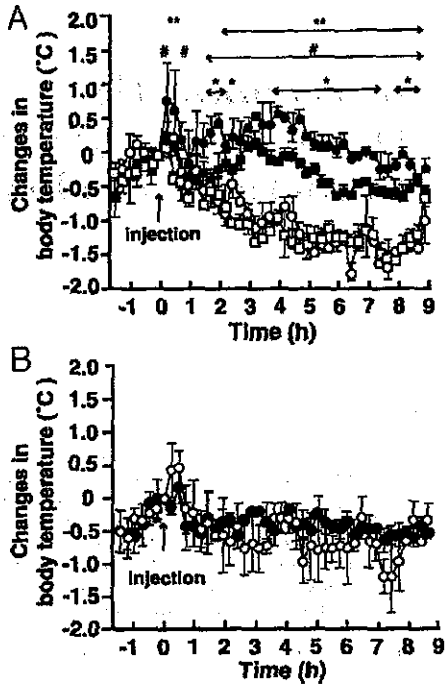


FIG. 1. Effects of *IL-1α/β* or *IL-6* deficiency on fever development after injection with IL-1α (1 μg/kg BW, iv injection). The body temperatures relative to that at the time of IL-1α injection are shown. A, IL-1α-injected wild-type mice (n = 4; ■); saline-injected wild-type mice (n = 4; □); IL-1α-injected *IL-1α/β*-deficient mice (n = 3; ●); and saline-injected *IL-1α/β*-deficient mice (n = 3; ○). B, IL-1α-injected *IL-6*-deficient mice (n = 3; ●); and saline-injected *IL-6*-deficient mice (n = 3; ○). Averages ± SD are shown. *, $P < 0.05$, IL-1α-injected wild-type mice *vs.* IL-1α-injected *IL-1α/β*-deficient mice; #, $P < 0.05$, IL-1α-injected *IL-1α/β*-deficient mice *vs.* saline-injected *IL-1α/β*-deficient mice; **, $P < 0.05$, IL-1α-injected wild-type mice *vs.* saline-injected wild-type mice.

## Results

### *Febrile response to IL-1α in IL-1α/β-deficient and IL-6-deficient mice*

Wild-type, *IL-1α/β*-deficient, and *IL-6*-deficient mice were injected iv with IL-1α, and the resulting febrile responses were examined. The measurement of the temperature started at 0930 h, and IL-1 was injected at 1100 h. The body temperature of untreated mice gradually decreased from 0930 to 1900 h and again rose after that, reflecting the circadian temperature rhythm. The preinjection body temperatures for each experimental group were the same: IL-1-injected wild-type mice, 37.6 ± 0.2; saline-injected wild-type mice, 37.5 ± 0.4; IL-1-injected *IL-1α/β*-deficient mice, 37.6 ± 0.1; saline-injected *IL-1α/β*-deficient mice, 37.3 ± 0.3; IL-1-injected *IL-6*-deficient mice, 37.4 ± 0.3; and saline-injected I *IL-6*-deficient mice, 37.6 ± 0.3. As shown in Fig. 1A, when *IL-1α* was administered, wild-type mice showed significantly elevated body temperatures (at 30 min and from 2 h 15 min to 8 h 45 min after injection), compared with saline-injected wild-type mouse controls (**, $P < 0.05$). IL-1-injected *IL-1α/β*-deficient mice also showed a febrile response similar to wild-type mice: significantly elevated temperature was observed at 15,